A phase-space representation of nucleon-nucleon potentials*

D. Weber[1,2], *H. Feldmeier*[1,2,3], *and T. Neff*[1,2]

[1]EMMI, Darmstadt, Germany; [2]GSI, Darmstadt, Germany; [3]FIAS, Frankfurt, Germany

Effective realistic nucleon-nucleon (NN) potentials that do not scatter to high momenta contain momentum dependent contributions. The Argonne potential [1] transformed by means of the Unitary Correlation Operator Method [2], for example, has a quadratic momentum dependence. Interactions arising from the Similarity Renormalization Group (SRG) method [3] show a more complicated momentum dependence, which is, however, not transparent as these potentials are constructed directly in matrix element representation.

To investigate the momentum dependence of NN potentials given by matrix elements, we use the phase-space representation introduced by Kirkwood [4]. In this representation the phase-space distribution $f_{ps}(\vec{r},\vec{p})$ for a density operator ρ and the representation $O_{ps}(\vec{r},\vec{p})$ of an operator $\mathcal{O}$ are given by

$$f_{ps}(\vec{r},\vec{p}) = (2\pi)^{3/2} \left\langle \vec{r}\right|\rho\left|\vec{p}\right\rangle\left\langle \vec{p}\right|\vec{r}\left\rangle \right. \quad (1a)$$

$$O_{ps}(\vec{r},\vec{p}) = (2\pi)^{3/2} \left\langle \vec{r}\right|\mathcal{O}\left|\vec{p}\right\rangle\left\langle \vec{p}\right|\vec{r}\left\rangle, \right. \quad (1b)$$

such that

$$\left\langle \mathcal{O} \right\rangle = \mathrm{Tr}\,(\rho\mathcal{O}) \int \mathrm{d}^3r\mathrm{d}^3p\, f^*_{ps}(\vec{r},\vec{p}) \cdot O_{ps}(\vec{r},\vec{p}). \quad (1c)$$

For a potential given in partial wave matrix elements $\left\langle kLM;S;T\left|\mathbf{V}\right|pLM;S;T\right\rangle$, with the momentum quantum numbers L and M and spin and isospin S and T, Eq. (1b) can be rewritten as

$$V_{ps}(\vec{r},\vec{p}) = 4\pi e^{-i\vec{r}\vec{p}} \sum_{L,M} i^L Y^L_M(\hat{\vec{r}}) {Y^L_M}^*(\hat{\vec{p}}) \times \int_0^\infty \mathrm{d}k k^2 \left\langle kLM;S;T\left|\mathbf{V}\right|pLM;S;T\right\rangle j_L(rk), \quad (2)$$

where Y^L_M is a spherical harmonic and j_L a spherical Bessel function. We describe the angular part of $V_{ps}(\vec{r},\vec{p})$ by an expansion in Legendre polynomials $P_\Lambda(\hat{\vec{r}}\cdot\hat{\vec{p}})$:

$$V_{ps}(\vec{r},\vec{p}) = \sum_\Lambda i^\Lambda V^\Lambda_{ps}(r,p) P_\Lambda(\hat{\vec{r}}\cdot\hat{\vec{p}}). \quad (3)$$

Fig. 1 shows the first terms of this expansion calculated by means of Eq. (2) from the matrix elements of different potentials, namely a local potential $V(\mathbf{r})$, a potential with quadratic momentum dependence, and a potential with quadratic angular momentum dependence. For the local potential, $V_{ps}(\vec{r},\vec{p})$ is just $V(r)$ and the phase-space representation does not depend explicitely on p and the angle between $\vec{r}$ and $\vec{p}$. For the quadratic momentum dependent potential $\mathbf{V} = \frac{1}{2}\left(\vec{\mathbf{p}}^{\,2}V(\mathbf{r}) + V(\mathbf{r})\vec{\mathbf{p}}^{\,2}\right)$ the phase-space representation shows a characteristic quadratic momentum dependence for $\Lambda = 0$ and a $\Lambda = 1$ contribution reflecting the fact that $\vec{\mathbf{r}}$ and $\vec{\mathbf{p}}$ do not commute. All higher Λ-contributions vanish. $V_{ps}(\vec{r},\vec{p})$ of the quadratic angular momentum potential contains terms up to $\Lambda = 2$. Potentials with more complicated momentum dependencies, for example from a SRG transformation, would create contributions also for higher Λ.

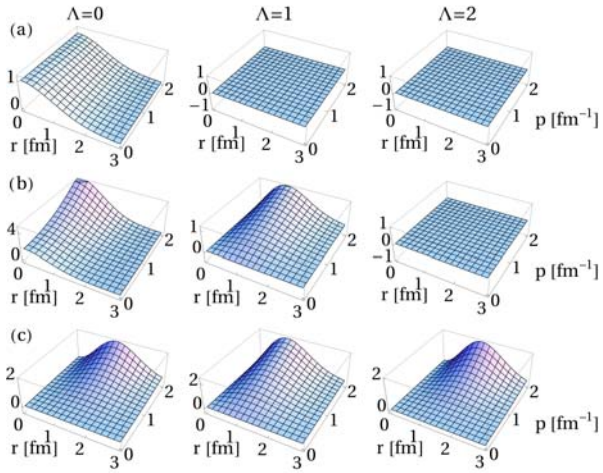

Figure 1: Phase-space representation $V^\Lambda_{ps}(r,p)$ in arbitrary units for (a) $\mathbf{V} = V(\mathbf{r})$, (b) $\mathbf{V} = \frac{1}{2}\left(\vec{\mathbf{p}}^{\,2}V(\mathbf{r}) + V(\mathbf{r})\vec{\mathbf{p}}^{\,2}\right)$, (c) $\mathbf{V} = V(\mathbf{r})\,\vec{\mathbf{L}}^2$. $V(r) = e^{-\frac{r^2}{2\,\mathrm{fm}^2}}$.

These results show that the phase-space representation is able to visualize the (non-) local structure of a potential. In further studies we plan to employ this method to investigate the momentum dependence of various realistic NN potentials given in matrix representation.

References

[1] R. B. Wiringa, V. G. J. Stoks and R. Schiavilla, Phys. Rev. C, 51, 38-51 (1995)

[2] R. Roth, T. Neff and H. Feldmeier, Prog. Part. Nucl. Phys., 65, 50 (2010)

[3] S. K. Bogner, R. J. Furnstahl and R. J. Perry, Phys. Rev. C, 75, 061001 (2007)

[4] J. G. Kirkwood, Phys. Rev., 44, 31 (1933)

* Supported by the Helmholtz Alliance EMMI

The ^{12}C continuum in a microscopic coupled channel calculation*

T. Neff[1,2] *and H. Feldmeier*[1,2,3]

[1]GSI, Darmstadt, Germany; [2]EMMI, Darmstadt, Germany; [3]FIAS, Frankfurt, Germany

For the description of scattering processes and resonances a proper treatment of the continuum is necessary. To achieve such a description in a microscopic many-body approach one has to connect compact configurations that describe the internal part of the wave function with external cluster configurations representing the open channels.

We have developed such an approach within fermionic molecular dynamics (FMD). FMD uses a wave-packet basis that allows to describe the internal parts of the wave function and the external cluster channels on equal footing. The matching to the asymptotic behavior as given by two point-like clusters interacting only via Coulomb is performed in the microscopic R-matrix formalism.

As a first example we discuss the continuum states in ^{12}C. We previously studied ^{12}C in bound state approximation [1]. The focus was on the properties of the Hoyle state, which lies just above the ^{8}Be-^{4}He threshold. Whereas the bound state approximation is expected to work well for a very narrow resonance like the Hoyle state this is no longer true for other resonances like the second 2^+ state. The resonance position and width for this state could only be determined very recently by direct excitation with photons [2]. The existence and the nature of other states in the continuum is still hotly debated.

To address these questions we extend our calculations with a proper treatment of the continuum. Before doing the full FMD calculation a study within the microscopic α-cluster model has been performed. The microscopic cluster model with full antisymmetrization and employing a phenomenological two-body interaction proved to be successful in describing many properties of ^{12}C. In the internal region the Hilbert space is built from three-α configurations on a triangular grid. In the external region ^{8}Be-^{4}He configurations are added. The ^{8}Be eigenstates are obtained in bound state approximation by diagonalizating configurations up to 9 fm distance. Our results will have to be checked for convergence with respect to increasing the number of included ^{8}Be (pseudo-) states. Technically the challenge is related to the restoration of rotational symmetry. First the intrinsic wave functions for ^{8}Be have to be projected on good angular momentum. In a second step the ^{8}Be-^{4}He configurations (with different orientations of the ^{8}Be spin) have to be projected on total angular momentum. For solving the Schrödinger equation with the microscopic R-matrix method, Hamiltonian and norm kernels for the different channels have to be calculated.

In Fig. 1 the calculated phase shifts (from the diagonal matrix elements of the coupled-channel S-matrix) in the 0^+ and 2^+ channels are shown. We included here the ^{8}Be ground state and the first 2^+ state at 3 MeV. In the ^{12}C 0^+ channel the extremely narrow Hoyle state resonance at 300 keV is not resolved when scanning over the energy. Its resonance properties can be calculated by employing Gamow boundary conditions. A second 0^+ resonance at 4 MeV is related to the opening of the ^{8}Be(2^+) channel. As can be seen in the inelasticities (the magnitudes of the diagonal S-matrix elements) there is a strong coupling between the ^{8}Be(0^+) and ^{8}Be(2^+) channels. When adding additional ^{8}Be channels we observe additional resonances in the region above 4 MeV. This might explain the experimental observation of a very broad resonance at 10.3 MeV. In the ^{12}C 2^+ channel a resonance of ^{8}Be(0^+)-^{4}He nature at 1.5 MeV is found. In a next step we will calculate the $B(E2)$ transition strength distribution to compare with the experimental result [2]. Additional resonances again appear after crossing the ^{8}Be(2^+)-^{4}He threshold.

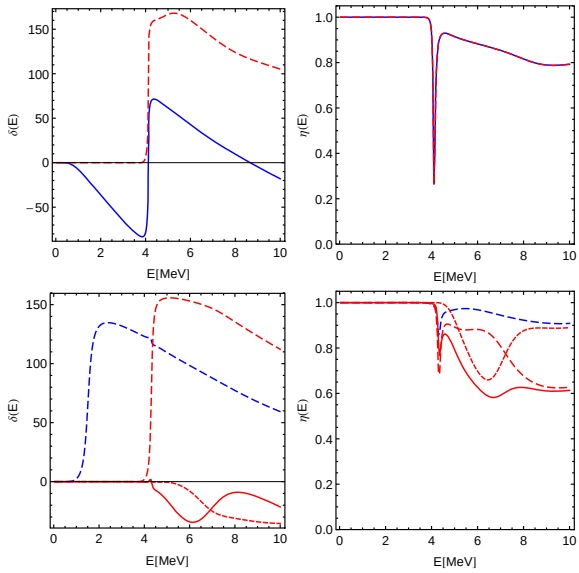

Figure 1: Phase shifts and inelasticity parameters for ^{8}Be-^{4}He scattering in 0^+ (top) and 2^+ channels (bottom). ^{8}Be(0^+) (blue lines) and ^{8}Be(2^+) (red lines) configurations are included.

References

[1] M. Chernykh *et al.*, Phys. Rev. Lett. **98**, 032501 (2007).

[2] W. R. Zimmermann *et al.*, Phys. Rev. Lett. **110**, 152502 (2013).

* Work supported in part by EMMI.

 doi:10.15120/GR-2014-1-THEORY-02

Theory of Nuclear Excitation and their Astrophysical Relevance *

N. Tsoneva[1,2] *and H. Lenske*[1,3]

[1]Institut für Theoretische Physik, Universität Gießen; [2]INRNE, 1784 Sofia, Bulgaria; [3]GSI Darmstadt

New modes of excitation in neutron-rich nuclei are described by an advanced Hartree-Fock-Bogoljubov (HFB) plus multiphonon approach.

Here, we report on recent spectroscopic studies in N=50 isotones based on the Quasiparticle-Phonon Model (QPM). The systematic calculations of dipole strength functions in these nuclei indicate enhanced $E1$ strength in the energy range from 6 to 10 MeV in agreement with the experimental observations [1]. From quasiparticle-random-phase approximation (QRPA) calculations, the energy region below E*$\leq$9 MeV is related to the pygmy dipole resonance (PDR) which total strength smoothly decreases with increasing charge number Z closely correlated with the thickness of the neutron skin. We point out that the QRPA is unable to account for the detailed description of the dipole strength function. However, three-phonon QPM calculations can reproduce the fine stucture of the latter fairly well as it follows from the comparison with the experiment [1]. Such precise knowledge of nuclear response functions is very important for the determination of photonuclear reactions cross sections for the astrophysics.

The microscopic strength functions have been implemented successfully into statistical reaction codes to investigate n-capture cross sections of astrophysical importance [2]. Our recent result on the n-capture cross section of the reaction ^{85}Kr(n,γ)^{36}Kr [2] is shown in Fig. 1. As seen, the microscopic calculations are in a very good agreement with the experimental data on the one hand and the HFB+combinatorial results on the other hand [2]. This agreement is confirming the predictive power of involved many-body theoretical methods like the QPM for exploratory investigations of n-capture reaction rates in hitherto experimentally inaccessible mass regions.

Recently, the fine structure of the $M1$-Giant Resonance (GR) in the nuclide ^{90}Zr was investigated [3]. Measurements performed in the range 7-11 MeV reveal a $M1$ resonance structure with centroid energy of 9 MeV and a summed strength of 4.5(4) μ_N^2. These data are fully reproduced in three-phonon QPM calculations [3]. The theoretical investigations which are presented in Fig. 2 indicate a strong increase of the contribution of the orbital part of the magnetic moment due to coupling of multiphononon states. Of special interest is the behavior of the M1 strength at higher energies close to and above the neutron-separation energy where the experimental accessibility is strongly reduced. For these regions, the theory predicts the existence

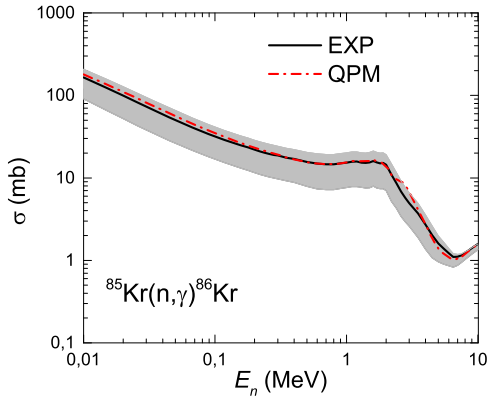

Figure 1: (color online) Cross section of $^{85}Kr^g(n,\gamma)^{86}$Kr calculated with TALYS using experimental dipole (in black) and QPM strength functions (in red) from Ref. [1]. The predicted uncertainties (shaded area) are derived from the experimental errors of the dipole strength function and from variations in the nuclear level density parameters.

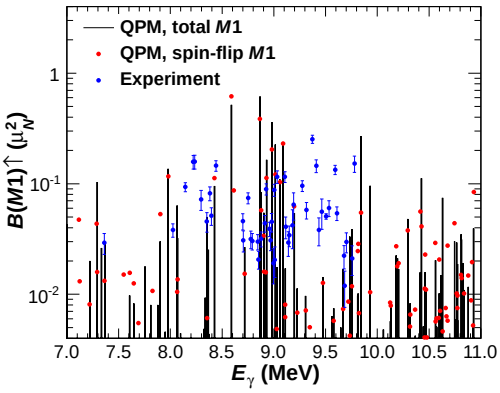

Figure 2: (color online) The measured M1 strength of discrete 1^+ levels in ^{90}Zr compared with three-phonon QPM predictions from Ref. [3].

of a strongly fragmented M1 strength with summed value of several μ_N^2. The latter is a very interesting finding which sheds light to the understanding of the long-standing problem with the quenching and dynamics of the M1 strength.

References

[1] R. Schwengner et al., Phys. Rev. **C 87**, 024306 (2013).

[2] R. Raut et al., Phys. Rev. Lett. **111**, 112501 (2013).

[3] G. Rusev et al., Phys. Rev. Lett. **110**, 022503 (2013).

* Work supported by the HIC for FAIR, GSI-JLU Giessen collaboration agreement, and BMBF Project No. 06GI9109.

Charged-current interactions for muon neutrinos in supernova*

A. Lohs[1,2], *G. Martínez-Pinedo*[1,2], *and T. Fischer*[3]

[1]Institut für Kernphysik (Theoriezentrum), Technische Universität Darmstadt, Darmstadt, Germany; [2]GSI-Helmholtzzentrum für Schwerionenforschung, Darmstadt, Germany; [3]Institute for Theoretical Physics, University of Wrocław, Wrocław, Poland

A core collapse supernova is emitting most of it's energy, up to 10^{53} erg in form of neutrinos of all flavours. The microphysics of neutrino transport is therefore an important ingredient to understand this astrophysical scenario. Present supernova simulations do not include charged current weak interaction for muon type neutrinos. These reactions are considered to be suppressed due to the large Q-value of the muon mass. As a consequence the spectra of muon and tau-type neutrinos is the same. Also the difference between ν_μ and $\bar{\nu}_\mu$ is minor. However, in the interior of a proto-neutron star chemical potentials and temperatures are large enough in the first seconds to allow for production of muons. Using conditions that were taken from 1D hydrodamical supernova simulations with full Boltzmann neutrino transport [1], we have derived and calculated the following reactions:

$$\nu_\mu + n \rightarrow p + \mu^- \qquad \nu_\mu + e^- \rightarrow \nu_e + \mu^-$$
$$\nu_\mu + \bar{\nu}_e + e^- \rightarrow \mu^- \qquad \bar{\nu}_e + e^- \rightarrow \bar{\nu}_\mu + \mu^-$$

The ν_μ-absorption on neutrons is calculated in analogy to absorption of electron-neutrinos [2, 3]. The three leptonic processes are derived similar to neutrino scattering on electrons [4, 5, 6]. We find that especially the absorption of ν_μ on neutrons and on electrons is a significant opacity source in the region where the neutrinos decouple energetically from the matter, at densities above 10^{13} g/cm^3.

We argue that charged current opacities for ν_μ will probably change the respective neutrino spectrum so it might differ significantly from the other heavy-neutrino flavours.

* Work supported GSI, HIC for FAIR, H-QM

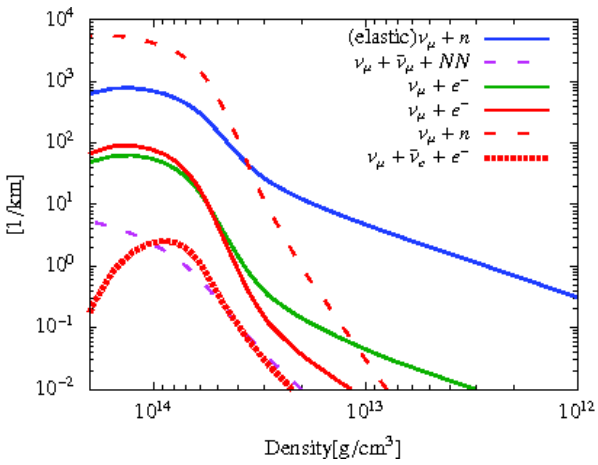

Figure 1: Spectraly averaged inverse mean free path of ν_μ

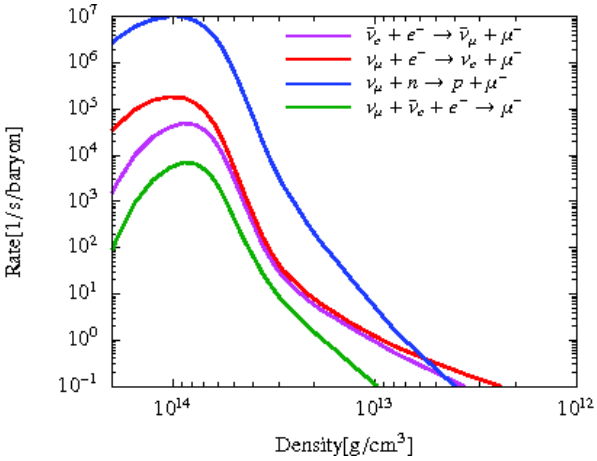

Figure 2: Rate of μ^--production per baryon per second

We also find that the production timescale of muons is comparably fast to the dynamical timescale. Muons will be in chemical equilibrium already at bounce. This should lead to the production of a positive net muon number in the core of the PNS. Also, once muons are present the charged current reactions contribute significantly to the equilibration of ν_μ of all energies. Eventually this might affect the deleptonization timescale of the PNS. The changes in the spectra could further be important for neutrino oscillations especially since the oscillations are sensitive to spectral differences. Finally we suggest that muonic charged current reactions should be implemented in future dynamical simulations of core collapse supernova to study their effects and to achieve an improved understanding of ν_μ spectra formation.

References

[1] T. Fischer, *et al.*, Astronomy and Astrophysics, **517** (2010), A80

[2] S. Reddy, M. Prakash, and J.M. Lattimer, Phys. Rev. D **58**, 013009 (1998)

[3] A.W. Steiner, M. Prakash, and J.M. Lattimer, Phys. Lett. B **509**, (2001), 10

[4] W.R. Yueh, J.R. Buchler, Astrophysics & Space Science, **41**, (1976), 221

[5] P.J. Schinder, S.L. Shapiro, ApJS, **50**, (1982), 23

[6] A. Mezzacappa, S.W. Bruenn, Astrophysical Journal, **410**, (1993), 740

 doi:10.15120/GR-2014-1-THEORY-04

Finite temperature pasta matter with the TDHF approximation *

B. Schuetrumpf[1], *M. A. Klatt*[2], *K. Iida*[3], *J. A. Maruhn*[1], *K. Mecke*[2], *and P.-G. Reinhard*[2]

[1]Institut für Theoretische Physik, Universität Frankfurt, D-60438 Frankfurt, Germany; [2]Institut für Theoretische Physik, Universität Erlangen-Nürnberg, D-91058 Erlangen, Germany; [3]Department of Natural Science, Kochi University, 2-5-1 Akebono-cho, Kochi 780-8520, Japan

Core-collapse supernova are relevant, e.g., for the synthesis of heavy nuclei and the formation of neutron stars. In such explosions, densities up to the nuclear saturation density as well as temperatures up to about $40\,\mathrm{MeV}$ are reached. If the mean nuclear density reaches about 10% of the nuclear saturation density, the matter forms rods to lower its surface energy. A further increase of density leads to slabs and even to inverted pasta, where the low density gas phase has the shape of the described pasta phases. Pasta shapes can be relevant e.g. for neutrino scattering which is important for the heat transport in a supernova or proto-neutron star.

The pasta matter is investigated here with the time-dependent Hartree-Fock approximation (TDHF) with the code explained in [1]. The wave functions on a 3d grid with periodic boundary conditions are evolved in time with finite time steps of $\Delta t = 0.1\,\mathrm{fm/c}$. For the present calculation a cubic box was taken with a lattice spacing of $1\,\mathrm{fm}$ and a box length of $16\,\mathrm{fm}$.

As initial conditions α-particles are distributed randomly in space keeping a minimal distance between them and in momentum space with a Maxwell-Boltzmann distribution. Free background neutrons are added as plane wave states with Fermi distribution of momenta. The setups are evolved in time until topological stability is reached. Then the temperature is roughly estimated with a Fermi gas approximation.

Fig. 1 exemplifies the emerging shapes, ordered by the mean density at which they appear. At low mean densities nearly spherical nuclei and "rods", infinitely long in one dimension, are found. "Rod(2)" and "rod(3)" are shapes where two or three rods are connected pointing in perpendicular directions. Note that for the slab shape which is doubly periodic and the rod(3) shape the gas and liquid phases are topologically identical. For higher volume fractions, the corresponding bubble shapes appear. All shapes can be uniquely classified by two simple scalar measures of the surface profile (Minkowski scalars), namely the integral mean curvature and the Euler number [2].

Figure 2 shows the map of the resulting pasta shapes. For the lowest temperature the shapes are well ordered. Pasta shapes exist for high temperatures at low densities. But the temperature for the transition to uniform matter decreases with increasing density.

*This work was supported by the BMBF under contract number 05P12RFFTG, DFG for the grant ME1361/11 and by Grants-in-Aid for Scientific Research on Innovative Areas through No. 24105008 provided by MEXT. The calculations have been performed on the cluster of the Center for Scientific Computing of the Goethe-Universität Frankfurt.

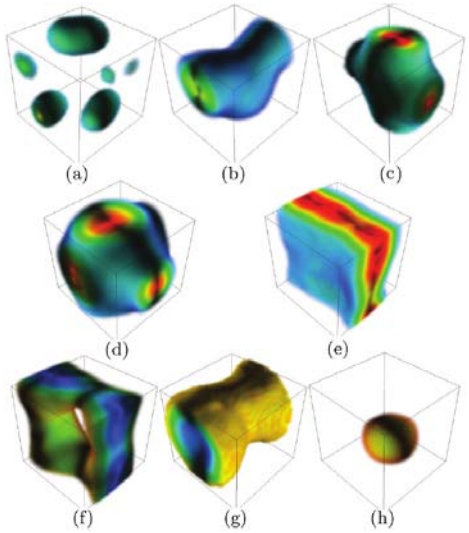

Figure 1: Shapes of pasta structures. Bubble shape illustrations show gas phase, indicated by the color-scale [from $0.03\,\mathrm{fm}$ (blue/light gray) to $0.12\,\mathrm{fm}$ (red/dark gray)]. (a) Sphere. (b) Rod. (c) Rod(2). (d) Rod(3). (e) Slab. (f) Rod(2) bubble. (g) Rod bubble. (h) Sphere bubble. This figure is taken from Ref. [2].

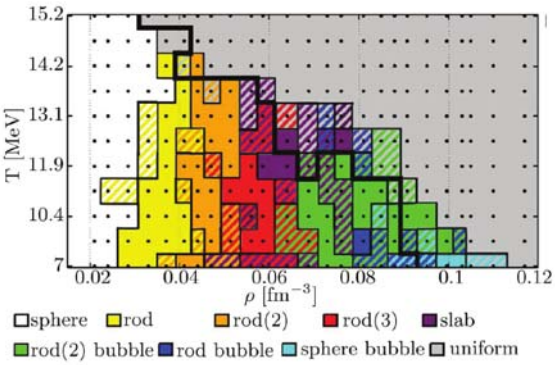

Figure 2: Map of pasta shapes for various temperatures and mean densities. Each dot represents two calculations. This figure is taken from Ref. [2].

References

[1] J. A. Maruhn, P.-G. Reinhard, P. D. Stevenson, and A. S. Umar, Comp. Phys. Comm. **to appear** (2014),arXiv:1310.5946

[2] B. Schuetrumpf, M. A. Klatt, K. Iida, J. A. Maruhn, K. Mecke, and P.-G. Reinhard, Phys. Rev. C **87**, 055805 (2013)

Symmetry energy of nuclear matter with liquid-gas phase transition and cluster formation*

S. Typel[1], *H.H. Wolter*[2], *G. Röpke*[3], *and D. Blaschke*[4,5]

[1]GSI Helmholtzzentrum für Schwerionenforschung, Darmstadt, Germany; [2]Ludwig-Maximilians-Universität München, Germany; [3]Institut für Physik, Universität Rostock, Germany; [4]Instytut Fizyki Teoretycznej, Uniwersytet Wrocławski, Poland; [5]Bogoliubov Laboratory for Theoretical Physics, JINR Dubna, Russia

The symmetry energy $E_{\rm sym}$ characterizes the energy change of strongly interacting matter when the isospin asymmetry δ is varied and all other independent quantities such as the baryon density n_B or temperature T are kept constant. The density dependence of $E_{\rm sym}$ is widely studied in experiment and theory since its precise form has a strong impact on the evolution of core-collapse supernovae and the structure and cooling of (proto) neutron stars.

For nuclear matter, the symmetry energy is usually calculated by assuming a uniform distribution of the constituent particles. However, dilute nuclear matter is not stable against density fluctuations and inhomogeneous matter on different length scales develops. E.g., at densities below saturation, clusters or macroscopic phases appear, which affect the actual density dependence of $E_{\rm sym}$. At finite temperatures, the symmetry free energy $F_{\rm sym}$ and the symmetry internal energy $U_{\rm sym}$ have to be distinguished. In addition, the results depend on the precise definition of the symmetry energy. These effects are studied in Ref. [1] using a relativistic density functional (RDF) approach with density dependent meson-nucleon couplings. The parameters of this phenomenological description are well constrained by fitting to properties of finite nuclei [2].

In nuclear matter at densities below saturation, the liquid-gas phase transition with coexisting low and high density phases was explicitly considered in the determination of the symmetry energy. As an example, the density dependence of $U_{\rm sym}$ for various temperatures is depicted in Figure 1 employing the finite difference formula, i.e. taking the difference of the energy per nucleon in pure neutron matter and in symmetric nuclear matter. This is equivalent to the standard definition using second derivatives with respect to the asymmetry δ only if the energy per nucleon is a quadratic function of δ. However, the former, finite difference definition gives more appropriate results for studying the variation of the energy with isospin. The liquid-gas phase transition leads to a substantial increase of the binding energy in symmetric nuclear matter due to the occurrence of a strongly bound high density phase. Hence a large finite symmetry energy is observed in particular at low temperatures even at very low densities.

In stellar matter, not only the strong interaction between the particles but also the electromagnetic interaction, which is artificially switched off in nuclear matter calculations, has to be considered. The charge neutrality condition is ensured by adding electrons and muons in proper amounts. The interplay between the surface tension and Coulomb repulsion leads to cluster formation on typical length scales with the size of nuclei. The RDF approach for nuclear matter has been extended to a generalized RDF with explicit cluster degrees of freedom [1, 2] including internal excitations of nuclei. Besides light (^{2}H, ^{3}H, ^{3}He, ^{4}He) and heavy nuclei ($A > 4$), nucleon-nucleon correlations in the continuum are included in an effective way [3]. They are necessary in order to reproduce the model-independent low-density benchmark, the virial equation of state. The formation and dissolution of cluster correlations are modeled by medium-dependent mass shifts, which are mainly driven by the action of the Pauli principle. With proper corrections for the effects of the Coulomb interaction, the symmetry energy in stellar matter exhibits similar features as in nuclear matter with liquid-gas phase transition.

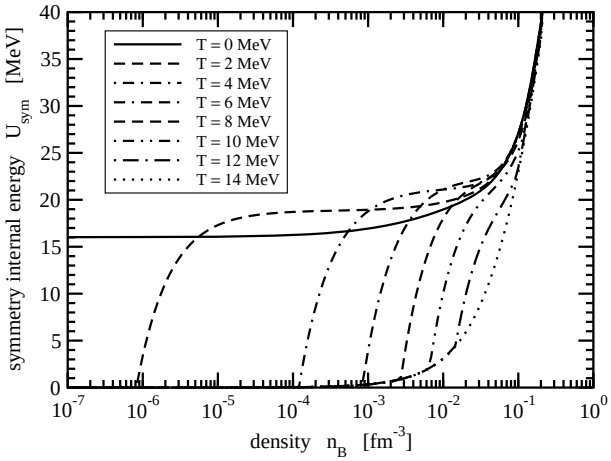

Figure 1: Density dependence of the symmetry internal energy of nuclear matter with liquid-gas phase transition for various temperatures.

References

[1] S. Typel, H.H. Wolter, G. Röpke and D. Blaschke, Eur. Phys. J. A 50 (2014) 17.

[2] S. Typel, G. Röpke, T. Klähn, D. Blaschke, and H.H. Wolter, Phys. Rev. C 81 (2010) 015803.

[3] M.D. Voskresenskaya and S. Typel, Nucl. Phys. A 887 (2012) 42.

*Work supported by the Helmholtz Association through the Nuclear Astrophysics Virtual Institute (VH-VI-417).

 doi:10.15120/GR-2014-1-THEORY-06

The chiral condensate in neutron matter *

T. Krüger[1,2], *I. Tews*[1,2], *B. Friman*[3], *K. Hebeler*[1,2], *and A. Schwenk*[2,1]

[1]IKP, Technische Universität Darmstadt, Darmstadt, Germany; [2]EMMI, GSI, Darmstadt, Germany; [3]GSI, Darmstadt, Germany

The chiral condensate is an order parameter for characterizing the chiral phase transition in dense and hot strongly interacting matter. Owing to the fermion sign problem, there are no first-principle QCD results for the phase diagram at low temperatures and high densities, the conditions probed in neutron stars. Recent observations of neutron stars with $2\,M_\odot$ masses provide general constraints on the equation of state (EOS) of cold strongly interacting matter, and put into question whether exotic phases that tend to soften the EOS are realized in neutron stars. At densities $n \lesssim n_0$, where $n_0 = 0.16\,\mathrm{fm}^{-3}$ denotes nuclear saturation density, the properties of nuclear systems have been studied systematically based on nuclear forces derived within chiral effective field theory and using renormalization group methods. In this work, we use chiral EFT interactions to study the chiral condensate as a function of density in neutron matter, based on perturbative calculations around the first-order Hartree-Fock energy.

The chiral condensate in neutron matter relative to the vacuum is given by [1]

$$\frac{\langle\bar{q}q\rangle_n}{\langle\bar{q}q\rangle_0} = 1 - \frac{n}{f_\pi^2}\frac{\sigma_{\pi N}}{m_\pi^2}\left(1 - \frac{3k_F^2}{10m_N^2} + \ldots\right) - \frac{n}{f_\pi^2}\frac{\partial}{\partial m_\pi^2}\frac{E_{\rm int}(m_\pi, k_F)}{N}\,. \quad (1)$$

The leading $\sigma_{\pi N}$ contribution to the chiral condensate in Eq. (1), which is due to the mass term in $E_{\rm free}/N$, is linear in density and is shown in Fig. 1 by the dashed line. For the density range shown in Fig. 1, where chiral EFT interactions can be applied with confidence, the kinetic energy contribution is only a 4% correction relative to the leading term, while relativistic corrections, indicated by the dots in Eq. (1), are negligible at these densities [1].

We calculate the explicit m_π dependence of nuclear forces by varying the value of the pion mass in the pion-exchange NN, 3N, and 4N interactions. At the NN level, we use the N^{3}LO potentials of Epelbaum, Glöckle, and Meißner [2] with cutoffs 450/500 and 450/700 MeV. With these NN interactions neutron matter is perturbative at the densities considered here [3, 4].

We find that nuclear interactions impede the restoration of chiral symmetry in neutron matter at zero temperature. The net effect of interactions remains below 10% for $n \lesssim 0.2\,\mathrm{fm}^{-3}$, but grows with increasing density. The dominant source of uncertainty is the $\sigma_{\pi N}$ term. We conclude that for moderate densities, say $n \lesssim 0.3\,\mathrm{fm}^{-3}$, a chiral phase transition in neutron-rich matter therefore seems unlikely, although we cannot exclude a strong first-order transition. For the densities considered here, we find a good convergence of the chiral condensate from N^{2}LO to N^{3}LO in chiral EFT. It would be very interesting to calculate the chiral condensate also for higher densities. While a systematic calculation in chiral EFT is difficult at densities much higher than $n = 0.2\,\mathrm{fm}^{-3}$, astrophysical observations provide valuable constraints.

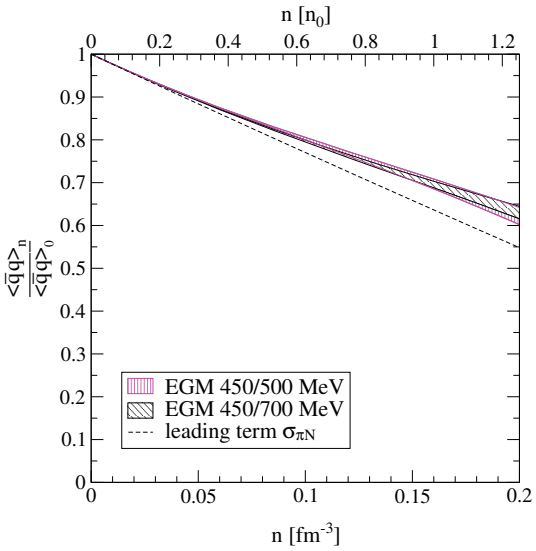

Figure 1: Chiral condensate $\langle\bar{q}q\rangle_n/\langle\bar{q}q\rangle_0$ as a function of density in neutron matter [1]. The dashed line is the leading pion-nucleon sigma-term contribution. The interaction contributions are obtained from the N^{3}LO neutron-matter calculation of Refs. [3, 4]. The bands for each NN potential include uncertainties of the many-body calculation, of the c_i couplings of 3N forces, and those resulting from the 3N/4N cutoff variation.

References

[1] T. Krüger, I. Tews, B. Friman, K. Hebeler, A. Schwenk, Phys. Lett. B276, 412 (2013).

[2] E. Epelbaum, W. Glöckle, and Ulf-G. Meißner, Eur. Phys. J. A 19, 401 (2004); Nucl. Phys. A 747, 362 (2005).

[3] I. Tews, T. Krüger, K. Hebeler, and A. Schwenk, Phys. Rev. Lett. **110**, 032504 (2013).

[4] T. Krüger, I. Tews, K. Hebeler, and A. Schwenk, Phys.Rev. C88, 025802 (2013).

* Work supported in part by EMMI, by the ERC Grant No. 307986 STRONGINT and by the DFG through SFB 634.

A low-energy effective model for quantum chromodynamics*

J. Berges[1] *and D. Gelfand*[1]
[1]University of Heidelberg, Heidelberg, Germany

In a low-energy effective model for quantum chromodynamics, we studied the real-time dynamics in a linear sigma model coupled to two light quark flavors. We found a dramatic amplification of quark production in the presence of highly occupied bosonic quanta for weak as well as strong effective couplings. For the mesonic sector we confirmed the existence of a turbulent scaling regime, known from previous studies of purely mesonic effective theories. Using for the first time real-time lattice field theory techniques with dynamical fermions in 3+1 dimensions, we demonstrated the failure of standard semiclassical descriptions based on the Dirac equation with a homogeneous background field to capture these phenomena [1].

To get a more detailed picture of quark dynamics and to test our approach we considered the range of validity of different methods: lattice simulations with male/female fermions, the mode functions approach and the quantum 2PI effective action with its associated kinetic theory. For strongly coupled quarks we found a rapid approach to a Fermi-Dirac distribution with time-dependent temperature and chemical potential parameters [2], while the mesons are still far from equilibrium.

We employed and improved the available real-time lattice techniques in order to investigate fermion–anti-fermion production in gauge theory, considering $1+1$ dimensional QED. In this non-perturbative approach the full quantum dynamics of fermions is included while the gauge field dynamics can be accurately represented by classical-statistical simulations for relevant field strengths. We computed the non-equilibrium time evolution of gauge invariant correlation functions implementing 'low-cost' Wilson fermions. Introducing a lattice generalization of the Dirac-Heisenberg-Wigner function, we recovered the Schwinger formula in $1+1$ dimensions in the limit of a static background field. We discuss the decay of the field due to the backreaction of the created fermion–anti-fermion pairs and apply the approach to strongly inhomogeneous gauge fields [3]. The latter allows us to discuss the striking phenomenon of a linear rising potential building up between produced fermion bunches after the initial electric pulse ceased and its decay, a phenomenon closely related to string-breaking in quantum chromodynamics.

Following these investigations we focused on the real-time dynamics of string breaking in quantum electrodynamics in one spatial dimension. A two-stage process with a clear separation of time and energy scales for the fermion–antifermion pair creation and subsequent charge separation leading to the screening of external charges was found [4]. Going away from the traditional setup of external static charges, we established the phenomenon of multiple string breaking by considering dynamical charges flying apart.

References

[1] J. Berges, D. Gelfand and J. Pruschke, Phys. Rev. Lett. **107** 061301 (2011)

[2] J. Berges, D. Gelfand and D. Sexty, Phys. Rev. D **89**, 025001 (2014)

[3] F. Hebenstreit, J. Berges and D. Gelfand, Phys. Rev. D **87**, 105006 (2013)

[4] F. Hebenstreit, J. Berges and D. Gelfand, Phys. Rev. Lett. **111** 201601 (2013)

* Work supported by HIC4FAIR/EMMI

 doi:10.15120/GR-2014-1-THEORY-08

Probing deconfinement with Polyakov loop susceptibilities *

Pok Man Lo[†1], *Bengt Friman*[1], *Olaf Kaczmarek*[2], *Krzysztof Redlich*[3], *and Chihiro Sasaki*[4]

[1]GSI, Darmstadt, Germany; [2]Universität Bielefeld, Bielefeld, Germany; [3]University of Wroclaw, Wrocław, Poland; [4]Frankfurt Institute for Advanced Studies, Frankfurt am Main, Germany

Deconfinement can be described by the spontaneous breaking of Z(3) center symmetry. The relevant quantities to study are the Polyakov loop and its susceptibilities. The Polyakov loop reflects the free energy of a static quark immersed in a hot gluonic medium. At low temperatures its thermal expectation value vanishes, signaling color confinement, while at high temperatures it is nonzero, resulting in a finite energy of a static quark and consequently the deconfinement of color. It is thus an order parameter for the deconfining phase transition.

The Polyakov loop susceptibility, on the other hand, represents fluctuations of the order parameter. It exhibits a peak at the transition temperature, and a width that signals the temperature window in which the phase transition takes place. While the basic thermodynamic functions of the SU(3) pure gauge theory, such as pressure and entropy, are well established within the lattice approach, the temperature dependence of the renormalized Polyakov loop and its susceptibilities are less clear. A careful study of these quantities will improve our understanding of the QCD phases.

In SU(3) gauge theory, the Polyakov loop is a complex-valued operator. One can therefore explore the fluctuations of the order parameter along the longitudinal (real) and transverse (imaginary) directions. However, the proper renormalization for these composite gluonic correlators remains ambiguous. One way to circumvent this problem is to consider the ratios of susceptibilities [1].

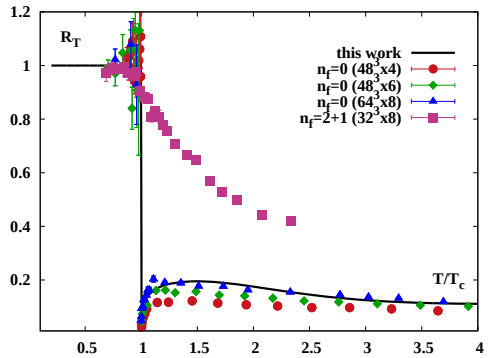

Figure 1: The ratio of Polyakov loop susceptibilities, $R_T = \chi_T/\chi_L$, in pure gauge system and in (2+1)-flavor QCD. The temperature is normalized to the (pseudo)critical value in each system. The lines show the results of the Polyakov loop model [2].

Fig. 1 shows the temperature dependence of the ratio of the transverse and longitudinal Polyakov loop susceptibilities, obtained in SU(3) gauge theory and in (2+1)-flavor QCD [2]. In the pure gauge limit ($N_f = 0$), the ratio R_T is discontinuous at T_c, and change only weakly with temperature on either side of the transition. This feature makes the ratio ideal for probing deconfinement. At high temperatures, the Z(3) symmetry is spontaneously broken. The pure gauge result indicates a small value for this ratio. In terms of an effective potential, this finding suggests that, around the global minimum associated with the symmetry-broken vacuum, the curvature in the transverse direction is much steeper than that in the longitudinal direction.

In the presence of light quarks, the Polyakov loop is no longer a true order parameter for deconfinement owing to the explicit breaking of the Z(3) symmetry. The ratio is smoothened and vary continuously across the pseudocritical temperature. One expects that the width of the crossover transition depends on the number of flavors and the values of quark masses. The value of R_T at high temperatures is found to deviate substantially from the pure gauge limit. An interpretation of this feature is still lacking.

We conclude that the ratio of Polyakov loop susceptibilities provides an excellent signal for the deconfinement phase transition. One immediate application of this work is to constrain the parameters used in effective models, thus providing a more realistic description of the QCD phase structure [2]. Further, more detailed lattice calculations are needed in order to obtain robust results for the gluonic correlation functions, as well as a better understanding of the systematic uncertainties.

References

[1] P. M. Lo, B. Friman, O. Kaczmarek, K. Redlich, and C. Sasaki, Phys. Rev. D **88** (2013) 014506.

[2] P. M. Lo, B. Friman, O. Kaczmarek, K. Redlich, and C. Sasaki, Phys. Rev. D **88** (2013) 074502.

* Work supported in part by FIAS and EMMI.

† pmlo@gsi.de

QCD phase structure and conserved charge fluctuations in a chiral effective model*

P. Rau[1], *J. Steinheimer*[1], *S. Schramm*[1], *and H. Stöcker*[2]
[2]GSI, Darmstadt, Germany; [1]FIAS, Goethe University, Frankfurt

Using the well-established chiral effective model for QCD matter, which includes all known hadrons up to $m = 2.6$ GeV and quarks, this study examines the phase structure of QCD matter and fluctuations of conserved charges focussing on the chiral and deconfinement phase transition. At small baryochemical potentials the effective model shows a smooth cross over in both order parameters and, at larger potentials, does not give indications for the existence of a first order phase transition and a critical end point. Compared to lattice QCD and thermal model fits of experimental data the chiral transition from the effective model is in line with recent data (Fig. 1).

At the phase transition conserved charges show large fluctuations which can be measured by susceptibility coefficients χ. Baryon number fluctuations are largely suppressed by the finite volume of hadrons and the suppressive particle interactions with vector fields (Fig. 2). It shows that in the hadronic phase below T_c coupling strengths are of the order of the nucleon couplings. However, in the quark sector above T_c, large fluctuations found in lattice QCD restrain quark vector couplings close to zero and particles at $T > T_c$ are almost acting like an ideal gas. With this model a realistic equation of state has been compiled which can be used for studying heavy ion collisions in dynamic models as well as neutron star properties.

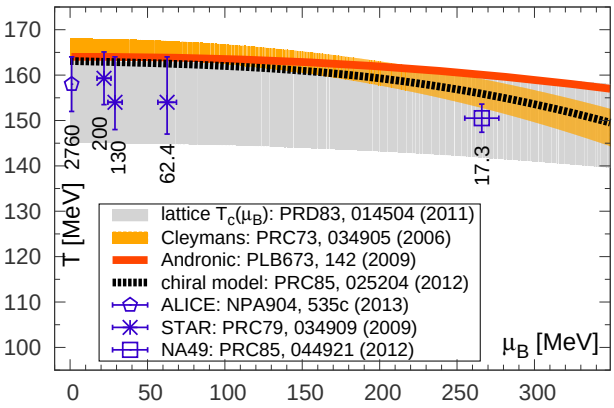

Figure 1: Chiral transition at small μ_B from lattice QCD (gray band) and from the chiral model (black line) contrasted to freeze-out curves from statistical and thermal model fits for SPS to LHC energies ($\sqrt{s_{\rm NN}}$ in GeV).

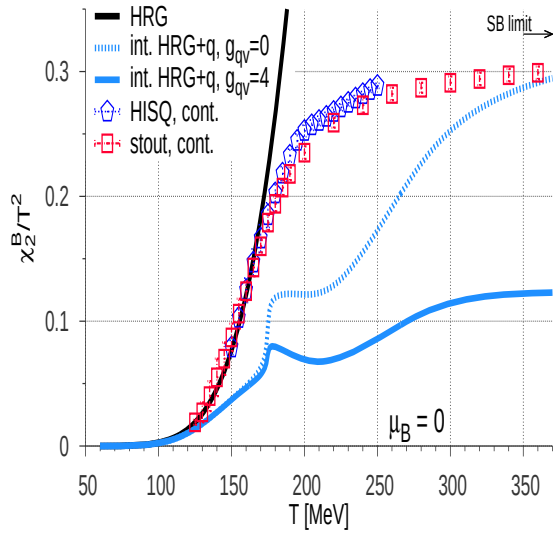

Figure 2: Second-order baryon number susceptibility of the hadron resonance gas (black line) and of the full model including hadrons and quarks (blue lines). Strong vector couplings suppress fluctuations and the Stefan-Boltzmann limit at high T may only be reached for vanishing quark vector couplings $g_{\rm qv}$ (dashed blue line).

Related publications in 2013:

1. P. Rau, J. Steinheimer, S. Schramm and H. Stöcker, *Chiral Hadronic Mean Field Model including Quark Degrees of Freedom*, J. Phys. G **40**, 085001 (2013).

2. P. Rau, J. Steinheimer, S. Schramm and H. Stöcker, *Conserved Charge Fluctuations in a Chiral Hadronic Model including Hadrons and Quarks*, arXiv:1308.4319 [hep-ph] (to be published in PLB).

* Work supported by HIC4FAIR

 doi:10.15120/GR-2014-1-THEORY-10

The role of fluctuations in the phase diagram of two color QCD*

N. Khan[1,2], *J. Pawlowski*[1,2], *F. Rennecke*[1,2], *and M. Scherer*[1,2]
[1]GSI, Darmstadt, Germany; [2]Universität Heidelberg, Germany

The investigation of the phase diagram of Quantum Chromodynamics (QCD) at finite temperature and density is an area of very active experimental and theoretical research [1] due to the existence of a variety of symmetry broken phases, the transitions between them and the presence of strong interactions. A straightforward application of lattice methods is inhibited by the property that for nonzero chemical potential the path integral measure of the QCD Lagrangian is complexAn instructive way to approach the full problem and to shed light on particular aspects is the investigation of deformations of QCD [2]. Generally, this can be achieved by changing e.g. mass parameters, symmetries or the field content. In this work, we will choose the latter two possibilities and study a theory similar to real QCD, however with two colors, $N_c = 2$, and two quark flavors $N_f = 2$. An appealing feature within this two-color two-flavor version of QCD is that, apart from the chirally broken mesonic phase of quark-antiquark pairs, it allows for the formation and (Bose-Einstein-) condensation of colorless diquarks, i.e. a bosonic baryon state. This results in a rich phase diagram with two dynamically competing order parameters.

In this work we employ a functional renormalization group (FRG) approach to an effective quark-meson-diquark model to study the phase diagram of two-color QCD. The FRG method is a suitable tool for the systematic study of (strongly) interacting field theories allowing for the formulation and computation of non-perturbative approximation schemes.The present work systematically extends the truncation scheme in Ref. [3] by taking into account the scale dependence of the wave function renormalizations as well as the renormalization of the Yukawa coupling between the quarks and the order parameter fields. Additional quantitative effects can be accessed systematically by extensions of the truncation scheme within the FRG. Here, we can monitor the quantitative corrections that are induced by the additional scale dependent quantities, namely the wave function renormalizations as well as the Yukawa interaction and study their impact on the phase diagram. Due to an alternative expansion scheme for the effective potential we gain direct access to the phenomenon of precondensation, a regime in the phase diagram where order occurs at intermediate scales but no order is found when all fluctuations are integrated out. In this way, we establish a refined picture of the FRG phase diagram for QC_2D, which is shown in Fig.1.

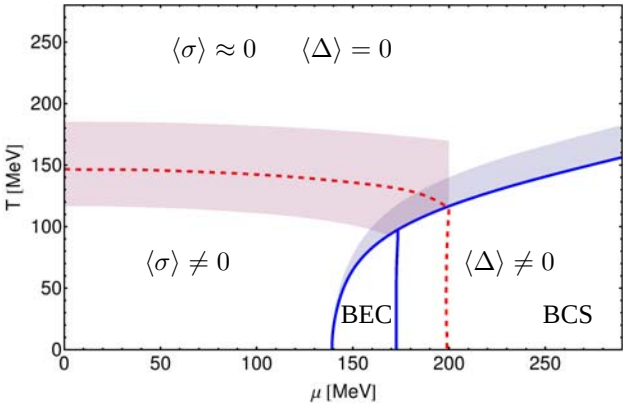

Figure 1: The phase daigram of QC_2D. μ is the baryon chemical potential in this plot.

The condensates are determined by the minimum of an order parameter potential, which is truncated to a one dimensional Taylor expansion up to six-point interaction terms. In addition, we have added a linear term in the chiral condensate σ, which causes chiral symmetry always to be broken, this is rooted in the fact that quarks have a small but finite current mass. At small temperatures and chemical potentials chiral symmetry is broken and quarks have a constituent mass of about 300 MeV. With increasing temperature the system undergoes a smooth crossover where chiral symmetry is nearly restored. The line and the shaded area in the left part of the figure mark the crossover and its width. At higher μ the system undergoes a second order phase transition at the onset of the diquark condensate Δ. At first the system is in BEC like state while at the limit of high chemical potentials the system spproaches a BCS like state. The line where the quark mass drops below the chemical potential indicates the region of the BEC-BSC crossover. The shaded area in the right part indicates the precondensation phase.

For the future this result is to be compared to lattice simulations, in order to evaluate our methods and truncation schemes.

References

[1] P. Braun-Munziger and J. Wambach, Rev. Mod. Phys. 81, 1031 (2009)

[2] L. von Smekal, Nucl. Phys. Proc. Suppl. 228, 179 (2012)

[3] N. Strodhoff, B.-J. Schaefer and L. von Smekal Phys. Rev. D85. 074007 (2012)

* Work supported by Helmholtz Alliance HA216/EMMI and by ERC-AdG-290623.

Higher order quark-mesonic scattering processes and the phase structure of QCD*

J. M. Pawlowski[1,2] *and F. Rennecke*[1,2]
[1]Universität Heidelberg, Germany; [2]GSI, Darmstadt, Germany

We study the chiral phase transition of two-flavor quantum chromodynamics (QCD) at finite temperature T and quark chemical potential μ [1]. At not too large chemical potential, the chiral dynamics in the vicinity of the phase boundary are driven by the lightest hadronic states, the pions and the sigma meson. Thus, in order to arrive at a quantitative picture of the matter sector of QCD, these mesonic degrees of freedom need to be taken into account accurately. We therefore employ a linear quark-meson model which captures spontaneous chiral symmetry breaking $SU(N_f)_L \otimes SU(N_f)_R \to SU(N_f)_V$. Quantum fluctuations are included by means of the functional renormalization group. The scale dependent effective action reads [2]:

$$\Gamma_k = \int_x \Big\{ iZ_{\psi,k}\bar{\psi}(\gamma_\mu\partial_\mu + \gamma_0\mu)\psi + \frac{1}{2}Z_{\phi,k}(\partial_\mu\phi)^2 + V_k(\rho) - c\sigma + h_k(\rho)\bar{\psi}(\gamma_5\vec{\tau}\vec{\pi} + i\sigma)\psi \Big\}, \quad (1)$$

where $\rho = \phi^2/2 = \vec{\pi}^2 + \sigma^2$. We systematically study the effect of higher order multi-meson as well as quark-antiquark multi-meson scattering processes on the chiral phase structure of QCD by expanding the effective potential $V_k(\rho)$ and the field-dependent Yukawa coupling $h_k(\rho)$ in powers of ρ. This corresponds to an expansion of the effective action Γ_k in terms of n-point functions. We observe that these higher order operators play a quantitatively important role for the chiral phase transition. Furthermore, the expansions of both, the effective potential and the Yukawa coupling, converge rapidly. This implies that we have good control over the quantitative precision of our results. For the effect of different parts of the truncation (1) on the phase boundary, see Fig. 1.

As a result of the explicit chiral symmetry breaking $-c\sigma$, which is directly related to finite current quark masses, we observe a crossover phase transition. The transition temperature/chemical potential in this case is not uniquely defined and we therefore compare different definitions of the phase boundary. Fig. 2 shows the resulting phase diagram. We find a crossover transition for $\mu < 291$ MeV. The large deviations in the transition temperatures between different definitions of the phase boundary indicate a very broad crossover. We note that the same is true for the curvature of the phase boundary at vanishing density. The crossover transition gets steeper towards the critical endpoint which we find at $(T_c, \mu_c) = (50, 291)$ MeV.

For the future this analysis can be used as a starting point for studies aiming towards full QCD, including baryonic degrees of freedom as well as the gauge sector of QCD.

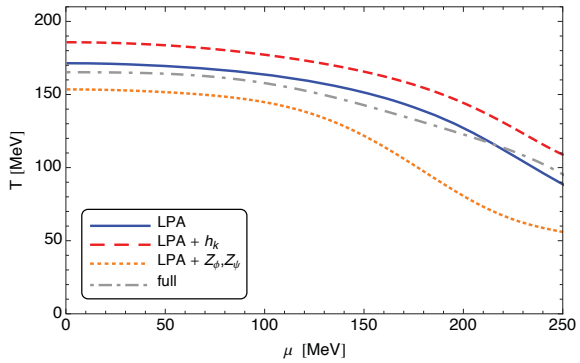

Figure 1: The crossover phase boundary for different truncations. LPA denotes the quark-meson model with only a running effective potential. The dot-dashed curve shows the full result of (1).

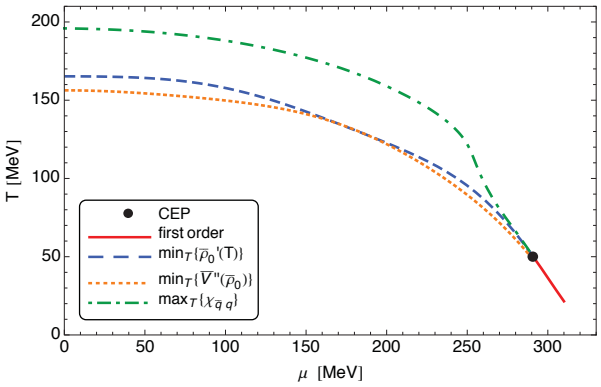

Figure 2: The phase diagram of the chiral transition of QCD. The crossover transition was extracted from three different quantities: the minimum of the effective potential (dashed), the quartic meson coupling (dotted) and the chiral susceptibility (dot-dashed).

References

[1] P. Braun-Munzinger and J. Wambach, "Colloquium: Phase diagram of strongly interacting matter", Rev. Mod. Phys. 81, p. 1031 (2009)

[2] J. M. Pawlowski and F. Rennecke, "Higher order quark-mesonic scattering processes and the phase structure of QCD", `hep-ph/1403.1179` (2014)

* Work supported by Helmholtz Alliance HA216/EMMI and by ERC-AdG-290623

 doi:10.15120/GR-2014-1-THEORY-12

Inhomogeneous condensation in nuclear matter*

Achim Heinz, Francesco Giacosa, and Dirk H. Rischke
ITP, Frankfurt am Main, Germany

Introduction

Spontaneous breaking of chiral symmetry is a nonperturbative phenomenon in the QCD vacuum as well as at low temperature and densities. Hadronic theories of the low energy regime have to take this into account [1]. Chiral symmetry breaking appears in the hadron spectrum as a mass splitting of so-called chiral partners.

A re-occurring topic in the literature is the possibility that the order parameter for the chiral transition is a function of spatial coordinate [2]. A fruitful Ansatz to describe inhomogeneous condensation is the chiral-density wave (CDW).

We re-investigate the question of inhomogeneous condensation at nonzero density in the extended Linear Sigma Model (eLSM) where the baryons are introduced as parity doublets [3, 4]. The eLSM successfully describes hadron vacuum phenomenology both in the meson and baryon sector, it is therefore a natural choice for non-zero density studies including the CDW [5].

Non-zero density study

In the two-flavor case, $N_f = 2$, the scalar and pseudoscalar mesons are described by the matrix

$$\Phi = (\sigma + \imath\eta_N)t_0 + (\vec{a}_0 + \imath\vec{\pi}) \cdot \vec{t}\,,$$

and the vector and axial-vector mesons by

$$V^\mu = \omega^\mu t_0 + \vec{\rho}^\mu \cdot \vec{t}\,, \quad A^\mu = f_1^\mu t_0 + \vec{a}_1^\mu \cdot \vec{t}\,,$$

where $\vec{t} = \vec{\tau}/2$, with the vector of Pauli matrices $\vec{\tau}$, and $t_0 = \mathbf{1}_2/2$. The model is invariant under the chiral group $SU(2)_R \times SU(2)_L$. The chiral condensate $\phi = \langle\sigma\rangle = Z f_\pi$ emerges upon spontaneous chiral symmetry breaking in the mesonic sector, where $f_\pi \simeq 92.4$ MeV is the pion decay constant and $Z \simeq 1.67$ is the wave-function renormalization constant of the pseudoscalar fields.

We now make the following Ansatz for the condensates, which is of the form of a chiral-density wave:

$$\langle\sigma\rangle = \phi\cos(2fx)\,, \langle\pi\rangle = \phi\sin(2fx)\,, \qquad (1)$$

In the limit $f \to 0$ we obtain the usual homogeneous condensation.

The baryons are introduced as two parity doublets Ψ_1 and Ψ_2, which transform according to the mirror assignment:

$$\Psi_{1,R} \to U_R\,\Psi_{1,R}\,, \qquad \Psi_{1,L} \to U_L\,\Psi_{1,L}\,, \qquad (2)$$

$$\Psi_{2,R} \to U_L\,\Psi_{2,R}\,, \qquad \Psi_{2,L} \to U_R\,\Psi_{2,L}\,. \qquad (3)$$

The mirror assignment allows for an additional chirally invariant mass term [6]:

$$m_0\left(\bar{\Psi}_{1,L}\Psi_{2,R} - \bar{\Psi}_{1,R}\Psi_{2,L} - \bar{\Psi}_{2,L}\Psi_{1,R} + \bar{\Psi}_{2,R}\Psi_{1,L}\right)\,. \qquad (4)$$

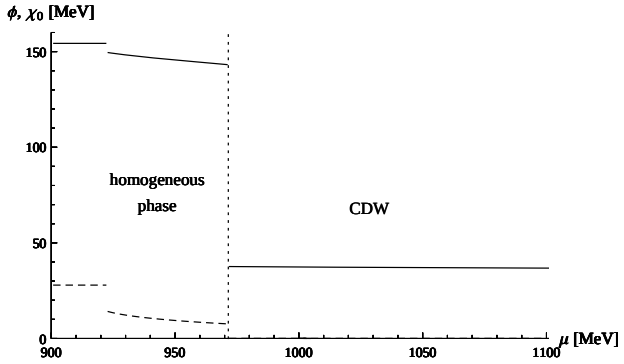

Figure 1: The condensates ϕ and $\bar{\chi}$ are shown as functions of μ.

In Fig. 1 the condensates ϕ and $\bar{\chi}$ are shown as functions of μ. For $\mu = 923$ MeV a first-order phase transition to the nuclear matter ground state takes place and at $\mu = 973$ MeV a transition to the CDW phase occurs. In terms of density, the onset of inhomogeneous condensation is at $2.4\rho_0$. Then, a mixed phase is realized between $2.4\rho_0$ to $10.4\rho_0$. However somewhere in the mixed phase the deconfinement phase transition should occur.

Outlook

Further studies of the model at zero and non-zero densities should be performed to test for general forms of inhomogeneous condensation. The eLSM should be extended to $N_f = 3$ in the baryon sector.

References

[1] S. Gasiorowicz et al. Rev. Mod. Phys. **41**, 531 (1969).

[2] A. B. Migdal, Rev. Mod. Phys. **50**, 107 (1978).

[3] D. Parganlija et al. Phys. Rev. D **82**, 054024 (2010);

[4] S. Gallas et al. Phys. Rev. D **82**, 014004 (2010).

[5] A. Heinz et al. arXiv:1312.3244 [nucl-th].

[6] C. DeTar et al. Phys. Rev. D **39**, 2805 (1989).

* Work supported by HGS-HIRe and HIC4FAIR.

Pions in a strong magnetic background *

G. Colucci† [1], *E. S. Fraga*[2], *and A. Sedrakian*[1]

[1]Institute for Theoretical Physics, J. W. Goethe-University, D-60438 Frankfurt am Main, Germany; [2]Instituto de Física, Universidade Federal do Rio de Janeiro, Caixa Postal 68528, Rio de Janeiro, RJ 21945-970, Brazil

We investigate the modification of the pion self-energy at finite temperature due to its interaction with a low-density, isospin-symmetric nuclear medium embedded in a constant magnetic background.

Nuclear matter in strong magnetic fields

The study of nuclear matter under strong magnetic fields has acquired a lot of attention during the last years in the contexts of heavy ion collision physics and lattice QCD [1]. In Ref. [2] we investigate some properties of isospin-symmetric nuclear matter in the limit of low density and temperature, embedded in a strong magnetic background. In particular, we compute the in-medium pion effective mass in the presence of a constant magnetic field to one loop. For this purpose, we consider fully relativistic chiral perturbation theory as a framework for our computation. This is needed to define consistently the fermion propagators in a magnetic background.

Pion self-energy in strong magnetic fields

The leading order interaction Lagrangian, which describe the low-energy phenomenology of nuclear matter, $\mathcal{L}^{(1)}_{\pi N}$, reads [3]

$$\mathcal{L}^{(1)}_{\pi N} = -\bar{\Psi}\left[\frac{g_A}{2f_\pi}\gamma^\mu\gamma_5\tau\cdot\partial_\mu\pi + \frac{1}{4f_\pi^2}\gamma^\mu\tau\cdot(\pi\times\partial_\mu\pi)\right]\Psi. \quad (1)$$

Here τ is the vector of Pauli matrices in isospin space, π is the isotriplet of pions, f_π the pion decay constant and g_A is the axial-vector coupling.

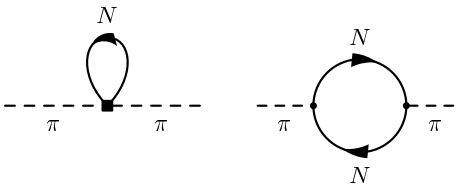

Figure 1: Diagrams contributing to the lowest-order in-medium pion self-energy.

The diagrams contributing to the pion self-energy from the Lagrangian (1) are shown in Fig. 1.

The effective pion mass is defined as:

$$m_\pi^{*\,2} = m_\pi^2 - \mathrm{Re}\,\Pi(m_\pi^{*\,2}, \mathbf{q}=0; \mathbf{B}) + (2n+1)|eB|\,, \quad (2)$$

where $\Pi(q)$ is the pion self-energy, $\mathbf{B}$ is the magnetic field and n is the index of the Landau level. The following results are computed within the lowest-Landau-level (LLL) approximation, which is valid for very intense magnetic fields.

Results

Fig. 2 displays our results for the pion effective mass, $\overline{m}_\pi$, as a function of the magnetic field, normalized to the trivial $|eB|$ shift in Eq. (2).

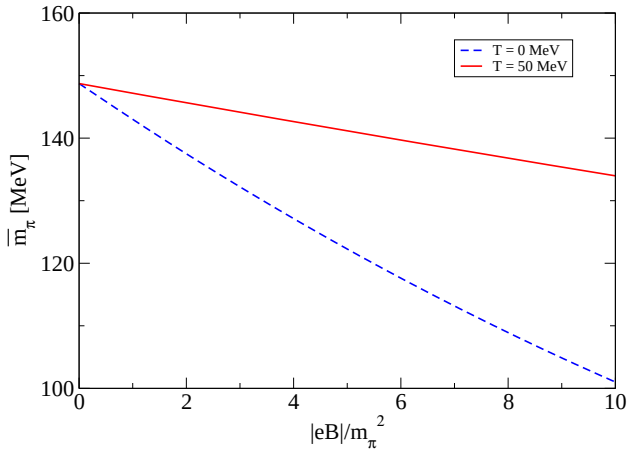

Figure 2: (Color online) Effective pion mass as a function of the magnetic field.

We find that the effective mass of the negatively charged pion drops by $\sim 10\%$ for a magnetic field $|eB| \sim m_\pi^2$, which favors pion condensation at high density and low temperatures.

References

[1] Dmitri Kharzeev, Karl Landsteiner, Andreas Schmitt, and Ho-Ung Yee. Strongly Interacting Matter in Magnetic Fields. *Lect.Notes Phys.*, 871:1–624, 2013.

[2] G. Colucci, E. S. Fraga and A. Sedrakian, Phys. Lett. B **728** (2014) 19

[3] R. Machleidt and D. R. Entem. Chiral effective field theory and nuclear forces. *Physics Report*, 503:1–75, June 2011.

* The work of GC was supported by the HGS-HIRe graduate program at Frankfurt University. The work of ESF was financially supported by the Helmholtz International Center for FAIR within the framework of the LOEWE program (Landesoffensive zur Entwicklung Wissenschaftlich-Ökonomischer Exzellenz) launched by the State of Hesse.

† colucci@th.physik.uni-frankfurt.de

 doi:10.15120/GR-2014-1-THEORY-14

Investigating the Transition Between Hydrodynamics and Transport *

D. Oliinychenko[1,3], *P. Huovinen*[2], *and H. Petersen*[1,2]

[1]Frankfurt Institute for Advanced Studies, Frankfurt am Main, Germany; [2]Institut für Theoretische Physik, Goethe Universität Frankfurt, Frankfurt am Main, Germany; [3]Bogolyubov Institute for Theoretical Physics, Kiev, Ukraine

Hybrid (hydrodynamics+transport) models are well suited to describe the dynamics of heavy ion collisions. However, there are common technical issues within such models that remain unsolved. In particular the established procedure of transforming hydrodynamics to transport by sampling particles according to the positive contributions of the Cooper-Frye equation [1] results in violating conservation laws. Typically, the hope is that small negative contributions will not influence the final results too much. The goal of our study is to explore the applicability range of this approach. We systematically investigate the behavior of Cooper-Frye negative contributions, in particular their dependence on hadron sort, collision energy (we consider the energy range of $\sqrt{s_{NN}} = 2-20$ GeV) and the criterion for the transition.

The negative contributions are calculated in two different ways: (I) hydro-based, assuming local thermal equilibrium and (II) particle-based, out of equilibrium. For this purpose many UrQMD events are generated and obtained particle trajectories are used to calculate the energy-momentum tensor $T^{\mu\nu}(t,x,y,z)$ on a space grid. In each grid cell the energy momentum tensor is transformed to the Landau rest frame (LRF) and a surface of constant LRF energy density is generated: $T^{00}_{LRF}(t,x,y,z) = \epsilon_0$, where ϵ_0 is an arbitrary parameter varied in the range 0.3 - 0.6 GeV/fm^3. Such surface mimics a typical transition surface that is used in hybrid models. Temperature and chemical potentials on the surface are obtained from a hadron gas equation of state. The negative contributions on this surface are calculated (I) from Cooper-Frye formula and (II) explicitly counting underlying particles.

The main results are as follows. The ratio of negative to positive contributions $x = [dN^-/dy]/[dN^+/dy]$ decreases with particle mass. It also decreases with collision energy as illustrated by Fig.1. In Fig. 1 one can also see that the value of x at midrapidity is 12 % at $E = 10$ AGeV while at $E = 160$ AGeV it is already around 3 % . It was found that x slightly grows with ϵ_0 and considerably increases at forward and backward rapidity if smooth transition surface is perturbed. This may be important for event-by-event calculations. Finally, x tends to be smaller for out of equilibrium "by particle" calculation than for Cooper-Frye calculation.

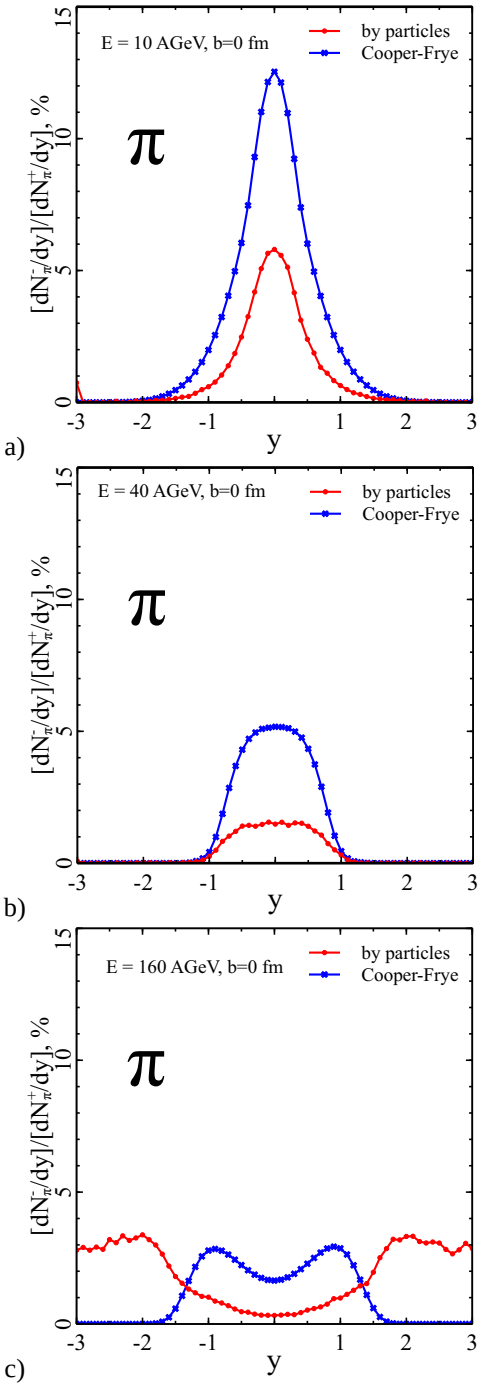

Figure 1: Negative contributions rapidity distribution for pions in central Au+Au collisions. $\epsilon_0 = 0.3$ GeV/fm^3. Crosses denote Cooper-Frye calculation while circles are "by-particle" calculation. Collision energy is a): $E = 10$ AGeV, b): $E = 40$ AGeV, c): $E = 160$ AGeV

References

[1] F. Cooper, G. Frye, Phys. Rev. D 10, 186, 1974

* Work supported by HIC for FAIR and Helmholtz-Nachwuchsgruppe VH-NG-822.

Collision Energy Evolution of Elliptic and Triangular Flow in a Hybrid Model*

J. Auvinen[1] *and H. Petersen*[1,2]

[1]Frankfurt Institute for Advanced Studies, Frankfurt am Main, Germany; [2]Institut für Theoretische Physik, Goethe Universität Frankfurt, Frankfurt am Main, Germany

We have studied the collision energy dependence of elliptic flow v_2 and triangular flow v_3 in Au+Au collisions within the energy range $\sqrt{s_{NN}} = 5 - 200$ GeV, utilizing a transport + hydrodynamics hybrid model [1,2]. The transport part is described by the Ultrarelativistic Quantum Molecular Dynamics (UrQMD), combined with an intermediate (3+1)-dimensional ideal hydrodynamical evolution phase using a chiral model equation of state. This approach provides a consistent framework for investigating both high-energy heavy ion collisions with negligible net-baryon density and a large hydrodynamically evolving medium, and the collisions at smaller energies with finite net-baryon density, where the hydrodynamics phase is very short-lived or does not exist at all.

The hybrid model reproduces the qualitative behavior of the experimentally measured elliptic flow (see Fig. 1(a)). While v_2 produced by hydrodynamics is considerably diminished at lower collision energies, this decrease is partially compensated by the transport dynamics, as shown in Fig. 1(b). The pre-hydrodynamics transport phase is of particular importance for understanding the collision energy evolution, while the hadronic rescatterings after the hydrodynamical phase contribute more systematically $\sim 10\%$ to the total flow at all energies. However, the viscous matter described by transport dynamics is unable to produce triangular flow, which consequently shows a significantly larger relative decrease in midcentral collisions with decreasing $\sqrt{s_{NN}}$ (Fig. 1(c)). Our conclusion is that the triangular flow provides the clearer signal for the formation of low-viscous fluid in heavy ion collisions.

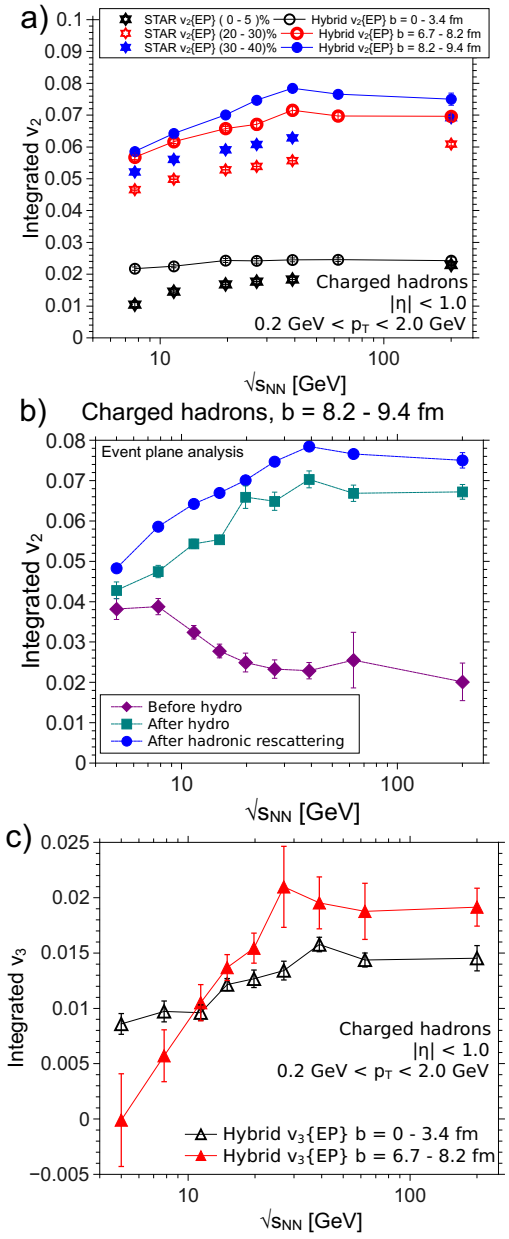

Figure 1: a): Integrated elliptic flow $v_2\{\mathrm{EP}\}$ for charged hadrons with $0.2 < p_T < 2.0$ at midrapidity $|\eta| < 1.0$ in Au+Au -collisions, for collision energies $\sqrt{s_{NN}} = 7.7 - 200$ GeV and three different impact parameter ranges, compared with the STAR data [3, 4]. b): Magnitude of $v_2\{\mathrm{EP}\}$ in midcentral collisions ($b = 8.2 - 9.4$ fm) at the beginning of hydrodynamical evolution (diamonds), immediately after the end of hydrodynamics phase (squares) and after the full simulation (circles). c): Integrated $v_3\{\mathrm{EP}\}$ in central collisions ($b = 0 - 3.4$ fm, open triangles) and midcentral collisions ($b = 6.7 - 8.2$ fm, solid triangles).

References

[1] J. Auvinen and H. Petersen, "Collision Energy Evolution of Elliptic and Triangular Flow in a Hybrid Model", PoS CPOD 2013 (2013) 034

[2] J. Auvinen and H. Petersen, "Evolution of elliptic and triangular flow as a function of collision energy in a hybrid model", Phys. Rev. C 88 (2013) 064908

[3] L. Adamczyk *et al.* [STAR Collaboration], "Inclusive charged hadron elliptic flow in Au + Au collisions at $\sqrt{s_{NN}}$ = 7.7 - 39 GeV", Phys. Rev. C 86 (2012) 054908

[4] J. Adams *et al.* [STAR Collaboration], "Azimuthal anisotropy in Au+Au collisions at $\sqrt{s_{NN}}$ = 200-GeV", Phys. Rev. C 72 (2012) 014904

* Work supported by HIC for FAIR and Helmholtz-Nachwuchsgruppe VH-NG-822. Computational resources have been provided by the Center for Scientific Computing (CSC) at Goethe Universität Frankfurt.

 doi:10.15120/GR-2014-1-THEORY-16

Initial conditions, hadronization and transport coefficients in heavy-ion collisions*

R. Marty[1], *E. Bratkovskaya*[1], *W. Cassing*[2], *and J. Aichelin*[3]
[1]FIAS, Frankfurt, Germany; [2]ITP, Giessen, Germany; [3]Subatech, Nantes, France

Introduction

The study of the properties of the Quark-Gluon Plasma (QGP) – formed in heavy-ion collisons – requires to understand how the initial quark and gluon distributions affect the final observables through the expansion and hadronization phases.

Initial conditions

The issue of initial conditions in relativistic heavy-ion collisions is a subject of intensive debate. Especially the assumption of thermal equilibrium after ∼1 fm/c is currently not supported by microscopic transport approaches. In our study we compare the Parton-Hadron-String Dynamics (PHSD) with the novel transport approach RSP (Relativistic quantum molecular dynamics for Strongly interacting matter with Phase transition or crossover) – based on the Nambu–Jona-Lasinio (NJL) model [1] – employing the same initial conditions from PHSD, which have a 'lumpy' energy density profile (see Fig. 1).

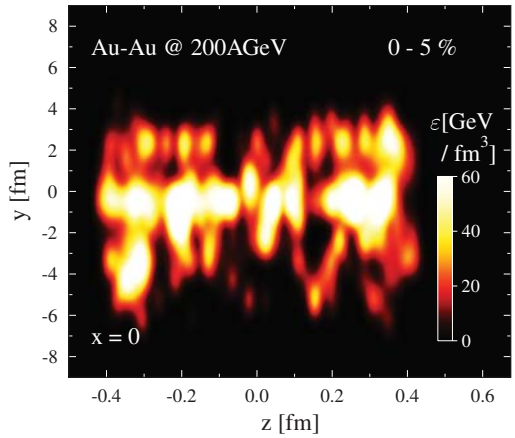

Figure 1: Initial energy density for cells in the local rest frame in the $y - z$ plane.

Comparison

Although we have the same initial energy density profile, the transport properties of bulk partonic matter in RSP and in PHSD are not the same [2]. The main difference between both approaches is that RSP uses light quarks which convert into hadrons using NJL cross sections, and that PHSD uses heavy partons (quarks and gluons) which combine into heavy hadrons with broad spectral functions which then decay into light hadrons.

The comparison of final hadronic observables (Fig. 2) shows that the initial parton distribution must be out of equilibrium in both approches (PHSD/RSP) in order to reproduce the multiplicity spectra dN/dp_T and $dN/d\eta$ and the elliptic flow v_2 for Au+Au at RHIC energies.

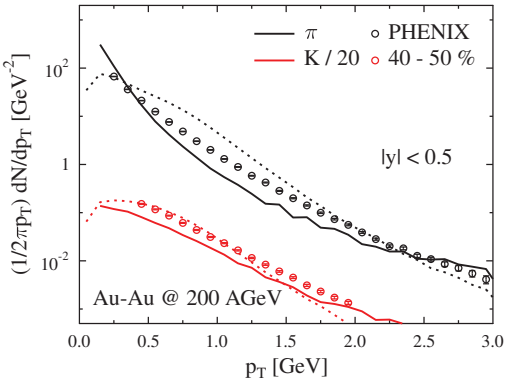

Figure 2: Transverse momentum distribution dN/dp_T of final charged pions and kaons in RSP (full lines) and PHSD (dashed lines).

Out of equilibrium

The conversion of fluid cells from one model to another – both out of equilibrium – keeps the interesting properties of the initial state: the anisotropy in momentum in p_T/p_z, the chemical mixture of species, and the particle density shift (for a given energy density in a cell, the equation of state gives a particle density which is not the one we really have in this cell in the out of equilibrium calculations).

Conclusion

This study shows the importance of non-equilibrium dynamics for the microscopic description of the quark-gluon-plasma created in heavy-ion collisions.

References

[1] R. Marty, J. Aichelin, Phys. Rev. C 87, 034912 (2013)

[2] R. Marty, E. Bratkovskaya, W. Cassing, J. Aichelin and H. Berrehrah, Phys. Rev. C 88, 045204 (2013)

* Work supported by the HIC for FAIR framework of the LOEWE program and the LOEWE-CSC for computational resources.

On- and off-shell heavy quark transport properties in the quark-gluon plasma*

H. Berrehrah[1], *E. Bratkovskaya*[1], *W. Cassing*[2], *P.B. Gossiaux*[3], *and J. Aichelin*[3]

[1]Frankfurt Institute for Advanced Studies; [2]Institut für Theoretische Physik, Giessen; [3]Subatech, Nantes, France

Within the aim of a dynamical study of on- and off-shell heavy quarks Q in the quark gluon plasma (QGP) - as produced in relativistic nucleus-nucleus collisions - we study the heavy quark collisional scattering on partons of the QGP and the underlying transport properties.

The collisional scattering cross sections σ^Q_{elas} are evaluated for perturbative partons (massless on-shell particles) and for dynamical quasi-particles (massive off-shell particles as described by the dynamical quasi-particles model "DQPM") using the leading order Born diagrams [1]. Figure 1 shows the elastic cross section of charm quark on a "u" quark as a function of $\sqrt{s}$, the energy in the c.m.s. of the collision for different temperatures. Comparing the DpQCD (Dressed pQCD) and IEHTL (Infrared Enhanced HTL) models where the partons have the DQPM pole masses in the first and are off-shell quasi-particles dressed by DQPM spectral functions in the second, we demonstrate that the finite width of the quasi-particles in the DQPM has little influence on σ^Q_{elas} except close to thresholds. The size of σ^Q_{elas} is dominated by the infrared regulator which in the finite temperature medium is determined by a dynamical gluon mass.

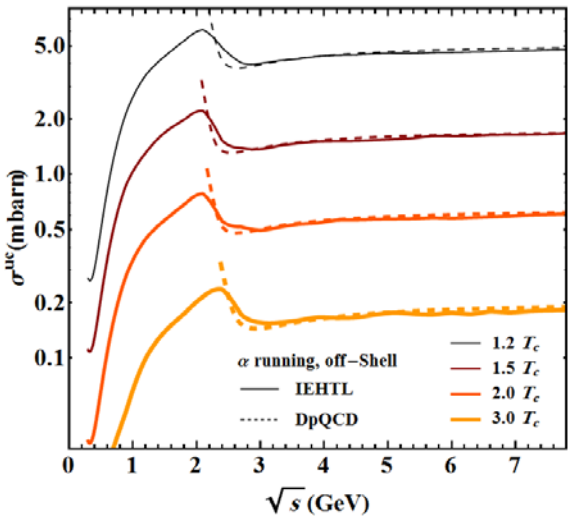

Figure 1: Elastic cross section of $uc \to uc$ for off-shell (solid lines) and on-shell partons (dashed lines) as a function of $\sqrt{s}$ for different temperatures.

Based on σ^Q_{elas} in a finite temperature medium [1], the on- and off-shell heavy quark dynamical collisional energy loss and transport coefficients are computed [2,3]. As an example, the charm drag coefficient is shown in figure 2 where both the on- and off-shell partons are employed. The Q momentum dependence of the drag is small in the non-perturbative models DpQCD/IEHTL compared to a pQCD calculations (HTL-GA with α constant or running). Our comprehensive comparison between perturbative and non-perturbative QCD based models shows out significant differences for the different Q transport characteristics. Nevertheless, our conclusion is that an explicit transport calculations in comparison to experimental data are needed to pin down the appropriate scenario, since the microscopic ingredients and the QGP background description are coupled and are specific to each model. The Q scattering cross sections and transport properties [1-3] will form the basis of a consistent study of the heavy quark dynamics in heavy-ion collisions at SPS, RHIC and LHC energies by implementing the partonic processes into the PHSD transport approach.

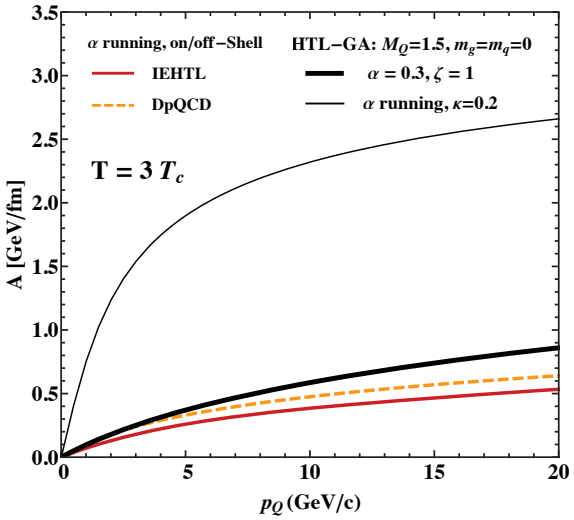

Figure 2: c-quark drag coefficient A from non-perturbative approaches DpQCD/IEHTL and the perturbative model HTL-GA as a function of the c-quark momentum.

References

[1] H. Berrehrah, E. Bratkovskaya, W. Cassing, P.B. Gossiaux, J. Aichelin and M. Bleicher, *arXiv:1308.5148 [hep-ph]*.

[2] H. Berrehrah, E. Bratkovskaya, W. Cassing, P.B. Gossiaux, J. Aichelin, *arXiv:1311.0736 [hep-ph]*.

[3] H. Berrehrah, E. Bratkovskaya, W. Cassing, P.B. Gossiaux, J. Aichelin., "Dynamical collisional energy loss and transport properties of on-shell and off-shell heavy quarks in vacuum and in the Quark-Gluon Plasma, *To be published*.

* Work supported by the HIC for FAIR framework of the LOEWE program and the LOEWE-CSC for computational resources.

 doi:10.15120/GR-2014-1-THEORY-18

Studies of jet quenching within a partonic transport model*

F. Senzel[1], *O. Fochler*[1], *J. Uphoff*[1], *Z. Xu*[2], *and C. Greiner*[1]

[1]Institut für Theoretische Physik, Johann Wolfgang Goethe-Universität, Max-von-Laue-Str. 1, D-60438 Frankfurt am Main, Germany; [2]Department of Physics, Tsinghua University, Beijing 100084, China

Jet quenching is one of the most promising phenomena for investigating hot and dense matter created in ultra-relativistic heavy-ion collisions at RHIC and LHC. Among the observables for characterizing the energy loss of a high-p_t parton are the suppression of particle spectra defined in terms of the nuclear modification factor R_{AA} [1] and the momentum imbalance A_J [2] of reconstructed di-jets. Both observables show a significant modification within heavy-ion collisions in comparison with p+p collisions [1, 2].

Within this report we show our progress in understanding jet quenching within the partonic transport model BAMPS [3], which numerically solves the 3+1D relativistic Boltzmann equation for quarks and gluons. While employing a running coupling $\alpha_s(t)$ evaluated at the momentum transfer of the respective, microscopic collision, BAMPS uses screened leading-order pQCD cross sections for the elastic $2 \to 2$ collisions and matrix elements calculated in a recently developed, improved Gunion-Bertsch approximation [4] for the inelastic $2 \leftrightarrow 3$ processes

$$\left|\overline{\mathcal{M}}_{X\to Y+g}\right|^2 = \left|\overline{\mathcal{M}}_{X\to Y}\right|^2 48\pi\alpha_s(k_\perp^2)\,(1-\bar{x})^2 \left[\frac{\mathbf{k}_\perp}{k_\perp^2} + \frac{\mathbf{q}_\perp - \mathbf{k}_\perp}{(\mathbf{q}_\perp - \mathbf{k}_\perp)^2 + m_D^2\,(\alpha_s(k_\perp^2))}\right]^2, \quad (1)$$

in which problems of the original GB matrix element [5] at non-zero rapidity of the emitted gluon are cured [4]. Since BAMPS is a classical transport model, the quantum Landau-Pomeranchuk-Migdal (LPM) effect is effectively implemented by a theta function $\theta(\lambda - X_{LPM}\,\tau_f)$ in the radiative matrix elements, where λ is the mean free path of the radiating parton and τ_f the gluon formation time.

After fixing the LPM parameter $X_{LPM} = 0.3$ by comparing to RHIC data, Fig. 1 shows the nuclear modification factor within BAMPS for gluons and quarks at LHC [6]. Additionally, the R_{AA} of charged hadrons obtained via a folding with AKK fragmentation functions is shown. The same X_{LPM} value for LHC simulations does not only describe the suppression of inclusive particle spectra, both at RHIC and LHC, nicely but also explains the momentum imbalance of reconstructed di-jets as shown in Fig. 2 [7].

Since BAMPS provides the full 3+1D microscopic information of all particles also studies of bulk observables like e.g. the elliptic flow v_2 are possible. Recently, these studies have shown that the *same* microscopic pQCD interactions as used in the jet quenching investigations lead to a sizable elliptic flow within the bulk medium [6].

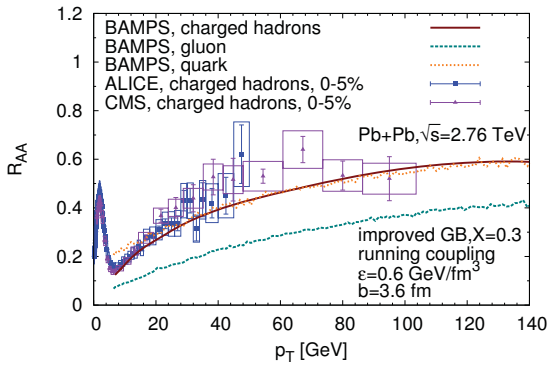

Figure 1: Nuclear modification factor R_{AA} of gluons, light quarks, and charged hadrons at LHC for PYTHIA initial conditions, a running coupling and LPM parameter $X_{LPM} = 0.3$ together with data of charged hadrons [1].

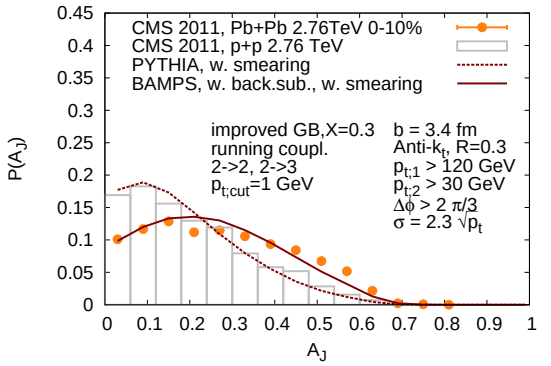

Figure 2: Momentum imbalance A_J of reconstructed jets in central Pb + Pb collisions at LHC for PYTHIA initial conditions, a running coupling and LPM parameter $X_{LPM} = 0.3$ together with data [2].

References

[1] ALICE Collaboration, Phys.Lett. **B720**, 52 (2013).

[2] CMS Collaboration, Phys. Lett. B **712** (2012) 176

[3] Z. Xu and C. Greiner, Phys.Rev. **C71**, 064901 (2005).

[4] O. Fochler et al., Phys.Rev. **D88**, 014018 (2013).

[5] J. Gunion and G. Bertsch, Phys.Rev. **D25**, 746 (1982).

[6] J. Uphoff et al., (2014), arXiv:1401.1364.

[7] F. Senzel et al., (2013), arXiv:1309.1657.

* Work supported by F&E Frankfurt/GSI, H-QM and HGS-HIRe.

Strange and heavy mesons in hot and dense nuclear matter: hadronic models and transport simulations for a road to FAIR*

D. Cabrera[1,2], *A. Ilner*[1,2], *J. M. Torres-Rincon*[3], *L. Tolos*[1,3], *J. Aichelin*[4], *E. Bratkovskaya*[1,2], *and W. Cassing*[5]

[1]FIAS, Frankfurt, Germany; [2]ITP, Frankfurt, Germany; [3]ICE (IEEC/CSIC), Bellaterra, Spain; [4]Subatech, Nantes, France; [5]ITP, Giessen, Germany

Introduction

Strage and heavy mesons probe interesting aspects of the strong interaction at extreme conditions, the different regions of the phase diagram being explored by experiments such as production reactions in nuclei, heavy-ion collisions (HICs) and the observation of macroscopic properties of neutron stars. Particularly, understanding their dynamics in the hadronic world is a crucial point to correctly analyse experimental information from HICs and perform realistic transport simulations. We study the properties of strange and heavy-flavoured mesons in a hot and dense nuclear medium within a selfconsistent coupled-channel approach based on the chiral Lagrangian.

Strange mesons in hot/dense matter

In the strangeness sector, we have completed a new determination of the in-medium scattering amplitudes and cross sections (such as $\bar{K}N \to \pi\Sigma$) in addition to the (off-shell) K and $\bar{K}$ spectral functions and quasi-particle properties, both at finite nuclear densities and temperatures, mimicking the expected scenario at FAIR experiments (c.f. Fig. 1). Our next step in this project is to implement our results in the IQMD and PHSD models, exploiting the successful collaboration between the transport groups of Nantes and FIAS-Frankfurt.

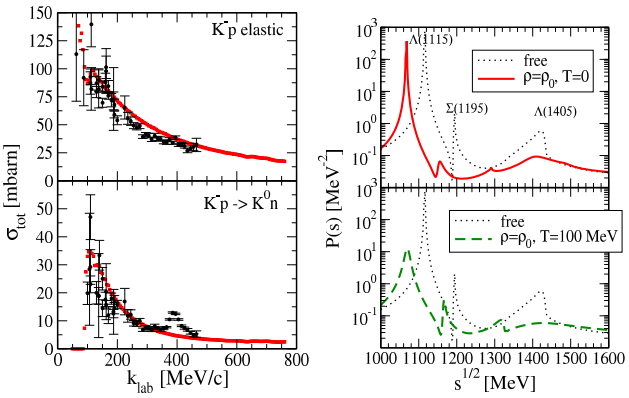

Figure 1: Left: K^-p elastic and $K^-p \to \bar{K}^0 n$ total cross sections (red squares: model). Right: Transition probability ($P \propto |T|^2$) for the K^-p elastic reaction at finite nuclear density (up) and temperature (down).

* Work supported by the HIC for FAIR framework of the LOEWE program and the BMBF project no. 05P12RFFCQ.

Heavy meson relaxation

In the heavy-flavour sector, our approach imposes partial-wave unitarity on the relevant scattering amplitudes (e.g. $D\pi$, $B\pi$), an essential requirement in order to extend the applicability of the low-energy theory (heavy-meson ChPT) to high temperatures $T \simeq m_\pi$. With a minimal set of parameters the unitarized theory dynamically generates the low lying heavy-light meson s-wave resonances ($D_{0,1}$, $B_{0,1}$) in good agreement with the available experimental data both in the charm and bottom sectors. Since a resonant interaction is bound to produce shorter thermalization times, accounting for this feature is important to produce a realistic estimation of the transport coefficients of heavy mesons in the hadronic phase of a heavy-ion collision (cf. Fig. 2).

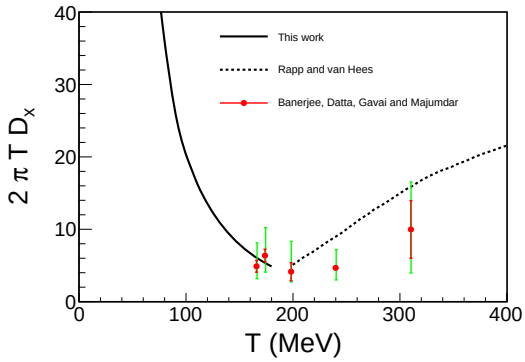

Figure 2: D-meson spacial diffusion coefficient around the crossover at $\mu_B = 0$.

References

[1] L. M. Abreu, D. Cabrera and J. M. Torres-Rincon, Phys. Rev. D **87** (2013) 3, 034019 [arXiv:1211.1331 [hep-ph]].

[2] L. Tolos, D. Cabrera, C. Garcia-Recio *et al.*, Nucl. Phys. A **914** (2013) 461 [arXiv:1211.7286 [nucl-th]].

[3] L. Tolos and J. M. Torres-Rincon, Phys. Rev. D **88** (2013) 074019 [arXiv:1306.5426 [hep-ph]].

[4] J. M. Torres-Rincon, L. M. Abreu, D. Cabrera *et al.*, to appear in Journal of Physics: Conference Series, arXiv:1312.3536 [hep-ph].

[5] D. Cabrera, L. M. Abreu, E. Bratkovskaya *et al.*, to appear in Journal of Physics: Conference Series, arXiv:1312.4343 [hep-ph].

[6] A. Ilner, D. Cabrera, P. Srisawad and E. Bratkovskaya, submitted to Nucl. Phys. A, arXiv:1312.5215 [hep-ph].

 doi:10.15120/GR-2014-1-THEORY-20

Heavy Quarks in Strongly Coupled Plasmas with Chemical Potential*

A. Samberg† [1,2] *and C. Ewerz*[1,2]

[1]Institut für Theoretische Physik, Universität Heidelberg, Philosophenweg 16, D-69120 Heidelberg, Germany;
[2]ExtreMe Matter Institute EMMI, GSI, Planckstraße 1, D-64291 Darmstadt, Germany

Introduction

In heavy ion collisions at RHIC and LHC, it is found that the produced quark–gluon plasma (QGP) is strongly coupled. We apply gauge/gravity duality [1] to study heavy quarks in strongly coupled non-Abelian plasmas. To approximate a dual description of QCD, we study non-conformal gauge theories by explicitly breaking the conformal invariance of the prototype AdS/CFT correspondence. As there is freedom in the way this breaking can be introduced, we study large classes of asymptotically AdS spacetimes, and try to uncover possible universal behavior common to all dual theories. Furthermore, to learn about the phase structure of strongly coupled gauge theories, and ultimately about parts of the QCD phase diagram, we include a chemical potential into our studies. Experimentally, this will be addressed *e. g.* in future FAIR experiments.

Specifically, we have computed the screening distance, the free energy, and a derived running coupling of heavy $Q\bar{Q}$ pairs moving in the strongly coupled plasmas described above. The methods used and results from studies in conformal theories are reviewed *e. g.* in [2].

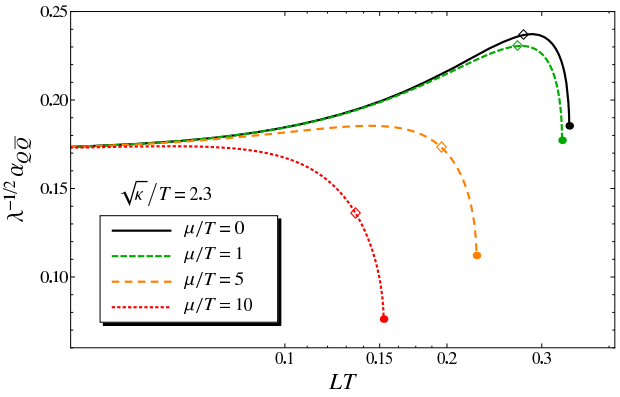

Figure 1: Running coupling $\alpha_{Q\bar{Q}}(L)$ in a non-conformal plasma at temperature T for varying values of the chemical potential μ. $\sqrt{\lambda}$ is a constant. At the endpoints of the curves, screening of the $Q\bar{Q}$ interaction due to the plasma takes over.

Free Energy and Running Coupling

We compute the free energy $F(L)$ of a bound $Q\bar{Q}$ pair with interquark distance L immersed in the medium. To get a handle on the effect of non-conformality on the interaction in more detail, we study the running coupling defined via the derivative of the free energy,

$$\alpha_{Q\bar{Q}}(L) \equiv \frac{3}{4} L^2 \frac{\mathrm{d}F(L)}{\mathrm{d}L} \,.$$

It is shown in Fig. 1. For small distances L, conformality is restored with $\alpha_{Q\bar{Q}}$ becoming constant, while for larger distances, both non-conformality and thermal effects lead to deviations of $\alpha_{Q\bar{Q}}$ from being constant. We have found a universal increase in $\alpha_{Q\bar{Q}}$ above the UV value due to non-conformality, both at vanishing and non-zero chemical potential μ. At still larger distances, thermal effects decrease $\alpha_{Q\bar{Q}}$. This pattern is also seen in QCD lattice data [3].

We have investigated the dependence of characteristic scales on temperature and chemical potential (*i. a.* the thermal drop-off scale L_{th} and the scale L_{max} where $\alpha_{Q\bar{Q}}$ assumes its maximum). At vanishing chemical potential, we have found that to leading order in our models with strong deformation away from conformality, $L_{\mathrm{max}} \sim \frac{c}{T^2}$, where c is the deformation parameter. This appears to be only weakly altered for $\mu > 0$. Generally, we have found that the effect of the chemical potential is relatively weak: also L_{th} varies more strongly under changes in T than in μ.

Comparing the free energy for non-zero μ to lattice data [4] where these are available, *i. e.* for $\mu/T \ll 1$, we find qualitative differences in the effect of the chemical potential that require further analysis. For our further studies, a very interesting outlook is to refine the comparison to lattice data to better characterize the commonalities and differences of holographic models for strongly coupled plasma and the QGP and to learn more about the nature of chemical potentials in holography.

Parts of these results were presented in [5], a more detailed account will be published elsewhere.

References

[1] J.M. Maldacena, Adv.Theor.Math.Phys. **2**, 231 (1998); S.S. Gubser, I.R. Klebanov, A.M. Polyakov, Phys. Lett. **B428**, 105 (1998); E. Witten, Adv.Theor.Math.Phys. **2**, 253 (1998).

[2] J. Casalderrey-Solana, H. Liu, D. Mateos, K. Rajagopal, U.A. Wiedemann, `arXiv:1101.0618`.

[3] O. Kaczmarek, F. Karsch, F. Zantow, P. Petreczky, Phys.Rev. **D70**, 074505 (2004).

[4] M. Döring, S. Ejiri, O. Kaczmarek, F. Karsch, E. Laermann, Eur.Phys.J **C46**, 179 (2006).

[5] C. Ewerz, A. Samberg, Proceedings of the Karl Schwarzschild Meeting 2013, Frankfurt, `arXiv:1312.5999`.

*Work supported by the Scientific Cooperation Agreement GSI–Heidelberg University.

† a.samberg@thphys.uni-heidelberg.de

Off-equilibrium photon production in heavy-ion collisions*

F. Michler[1], *H. van Hees*[1,2], *D. D. Dietrich*[1], *S. Leupold*[3], *and C. Greiner*[1]

[1]Goethe University Frankfurt, Max-von-Laue-Strasse 1, D-60438 Frankfurt, Germany; [2]FIAS, Ruth-Moufang-Strasse 1, D-60438 Frankfurt, Germany; [3]Institutionen för fysik och astronomi, Uppsala Universitet, Box 516, 75120 Uppsala, Sweden

As penetrating probes direct photons and dileptons provide insight into the hot and dense interior of matter created in heavy-ion collisions during its entire evolution. They are directly related with the electromagnetic-current correlation function in the strongly interacting medium. In this connection the most interesting signals are the p_t spectra of photons and dileptons and the invariant-mass spectra of dileptons from a thermalized medium to study the impact of the chiral phase transition in the QCD phase diagram to this current-correlation function.

However, to analyze experimental data on electromagnetic probes in heavy-ion collisions also a detailed understanding of all other "non-thermal" sources is important. In this study we investigate the contribution to the photon emission from the very early off-equilibrium state of the fireball created in heavy-ion collisions which are claimed to outshine the thermal emission from a QGP at high p_t in since here already contributions at order $\mathcal{O}(\alpha_{\mathrm{em}})$ of the electromagnetic coupling constant, which are forbidden in thermal equilibrium due to energy-momentum conservation, occur[1, 2, 3]. However, in this approach the photon rates are plagued by spurious vacuum-to-vacuum transition contributions which can not be renormalized in a proper way [4]. As shown in [5] this problem is related to "switching on and off" the electromagnetic interaction at finite times.

Motivated by these findings we investigate a toy model with quarks and antiquarks coupled to a classical time-dependent scalar field to mimick a time-dependent quark mass to investigate the pertinent emission of photons due to a possible chiral quark-mass shift in strongly interacting matter [6]. The advantage of this model is that it is compatible with current conservation and gauge invariance.

After analytically solving the Dirac equation for the quark-field operator coupled to a classical time-dependent scalar, we calculated the one-loop photon polarization tensor in 1$^{\mathrm{st}}$ order perturbation theory, employing the appropriate adiabatic switching of the electromagnetic interaction a la Gell-Mann and Low. We could explicitly show that this framework eliminates the spurious vacuum-to-vacuum transition contributions and allows to write the corresponding photon-emission rate as an absolute square, ensuring the positive definiteness of the photon-number density. For the realistic case of a smooth time dependence of the external field, mimicking a dropping quark-mass scenario by effectively switching the quark mass from its constituent value of $m_{\mathrm{c}} \simeq 0.35$ GeV to its bare value m_{b} for a duration of the off-equilibrium phase of $\tau = 1$ fm/c, the resulting time-integrated photon-momentum spectrum decays exponentially for large momenta and thus is UV integrable, leading to a finite photon yield from the underlying off-equilibrium process. Is has also been demonstrated that, e.g., using the adiabatic switch only for $t \to -\infty$ but not for $t \to \infty$ leads to an artificial enhancement of the photon-production rate by many orders of magnitudes due to spurious vacuum-to-vacuum transition contributions that cannot be properly interpreted as observable photon numbers.

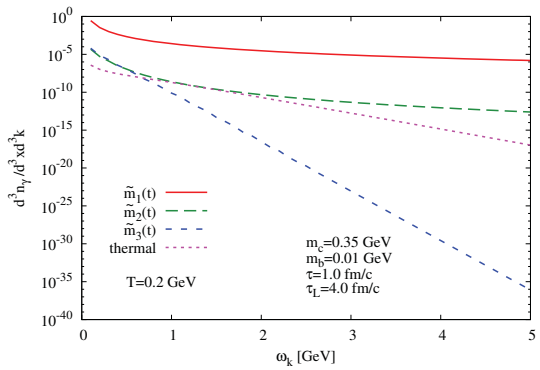

Figure 1: Comparison of the integrated off-equilibrium photon number for different mass-switching scenarios (instantaneous switch (solid line) and switching by a only 1st-order differentiable function (long-dashed line), leading implying the excitation of spurious modes and a UV divergent photon number, and a smooth switching function (short-dashed line) leading to a exponentially decreasing momentum spectrum and thus UV-finite photon-number densities with a photon spectrum from a thermalized QGP (lifetime 4 fm/c) at a temperature of 200 MeV.

References

[1] S.-Y. Wang and D. Boyanovsky, Phys. Rev. D **63**, 051702 (2001).

[2] D. Boyanovsky and H. de Vega, Phys. Rev. D **68**, 065018 (2003).

[3] D. Boyanovsky and H. J. de Vega, Nucl. Phys. A **747**, 564 (2005).

[4] E. Fraga, F. Gelis, and D. Schiff, Phys. Rev. D **71**, 085015 (2005).

[5] F. Arleo et al. (2004), `arXiv:hep-ph/0311131`.

[6] F. Michler, H. van Hees, D. D. Dietrich, S. Leupold, and C. Greiner, Annals Phys. **336**, 331 (2013).

* Work supported by HIC4FAIR/HGS-HIRe/HQM.

 doi:10.15120/GR-2014-1-THEORY-22

On finite volume effects in the chiral extrapolation of baryon masses

M.F.M. Lutz[1], *K. Schwarz*[1] *and R. Bavontaweepanya*[2], *C. Kobdaj*[2]

[1]GSI, Darmstadt, Germany; [2]Suranaree University of Technology, Nakhon Ratchasima, Thailand

We report on a comprehensive analysis of the available three flavour QCD lattice simulations of six different groups on the baryon octet and decuplet masses [1]. We obtained an accurate 12 parameter description of altogether more than 220 lattice data points, where we kept all data with pion masses smaller than 600 MeV. Our study extends previous works [4, 5, 6] and is based on the relativistic three-flavour chiral Lagrangian with baryon octet and decuplet degrees of freedom. The baryon self energies were computed in a finite box at N^{3}LO, where the physical masses are kept inside all loop integrals [1, 2]. The low-energy parameters were constrained by using large-N_c sum rules [3].

Accurate predictions for all relevant low-energy parameters were obtained. In particular we extracted a pion-nucleon sigma term of (39 ± 1) MeV and a strangeness sigma term of the nucleon of $\sigma_{sN} \simeq (4 \pm 1)$ MeV. The flavour SU(3) chiral limit of the baryon octet and decuplet masses was determined with (802 ± 4) MeV and (1103 ± 6) MeV. In our fits we used the empirical masses of the baryon octet and decuplet states as a constraint. That allowed us to perform independent scale settings for the various lattice data. We obtained results for the lattice scales that are compatible with previous estimates, but appear to be much more accurate. Detailed predictions for the baryon masses as currently evaluated by the ETM lattice QCD group are made.

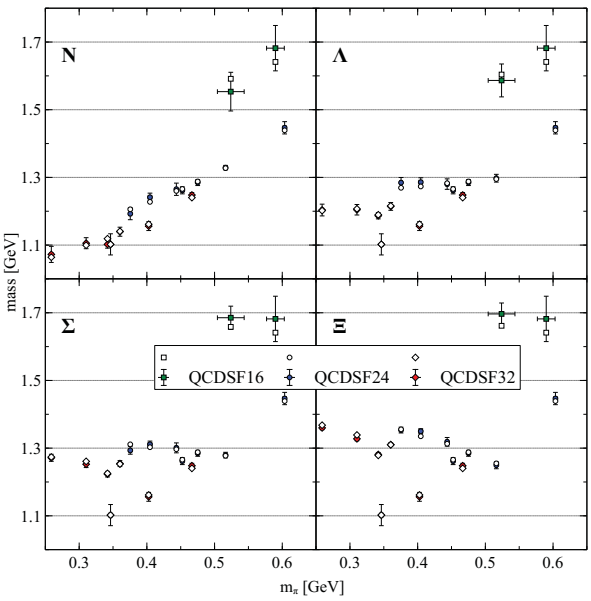

Figure 1: Baryon masses as a function of the pion mass as explained in the text. The open symbols are the result of our EFT analysis.

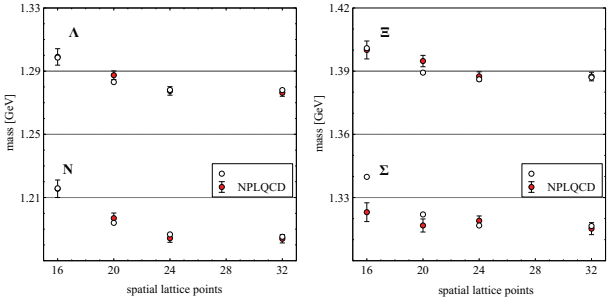

Figure 2: Baryon masses as a function of the pion mass as explained in the text. The open symbols are the result of our EFT analysis.

The 12 relevant low-energy parameter were determined by a global fit to all available lattice data with a $\chi^2/N \simeq 1.25$, which was shown to be dominated by a few outliers. It was emphasized that a stable fit with all parameters relevant at N^{3}LO is only possible upon the consideration of the lattice data at all available lattice volumes. In Fig. 1 we show a sample of our results where a comparison with QCD lattice simulations of the QCDSF-UKQCD group is provided. The description of the octet masses is excellent for all three different lattice sizes $16^3, 24^3$ and 32^3. In Fig. 2 the volume dependence of the baryon octet masses as studied by the NPLQCD group is scrutinized. Here our chi-square value is dominated by one outlier, the Σ mass on the smallest 16^3 lattice.

Our analysis points to some tension in the lattice data set on the baryon decuplet masses, in particular for the Δ mass of LHPC as compared to the predictions of HSC and PACS-CS.

References

[1] M. F. M. Lutz, R. Bavontaweepanya, C. Kobdaj, K. Schwarz, On finite volume effects in the chiral extrapolation of baryon masses, arXiv:1401.7805.

[2] A. Semke, M. F. M. Lutz, Baryon self energies in the chiral loop expansion, Nucl. Phys. A778 (2006) 153.

[3] M.F.M. Lutz, A. Semke, Large-N_c operator analysis of 2-body meson-baryon counterterms in the chiral Lagrangian, Phys. Rev. D83 (2011) 034008.

[4] A. Semke, M. F. M. Lutz, Quark-mass dependence of the baryon ground-state masses, Phys. Rev. D85 (2012) 034001.

[5] A. Semke, M. F. M. Lutz, Strangeness in the baryon ground states, Phys. Lett. B717 (2012) 242.

[6] M. F. M. Lutz, A. Semke, On the consistency of recent QCD lattice data of the baryon ground-state masses, Phys. Rev. D86 (2012) 091502.

doi:10.15120/GR-2014-1-THEORY-23

The salar-isovector sector in the extended Linear Sigma Model*

T. Wolkanowski[1], *F. Giacosa*[1], *and D. H. Rischke*[1]

[1]Institut für Theoretische Physik, Goethe-Universität Frankfurt am Main, Max-von-Laue-Str. 1, 60438 Frankfurt am Main, Germany

We study basic properties of scalar hadronic resonances within the so-called extended Linear Sigma Model (eLSM), which is an effective model of QCD based on chiral symmetry and dilatation invariance. In particular, we focus on the mass and decay width of the scalar-isovector state $a_0(1450)$ and perform a numerical study of the propagator pole(s) on the unphysical Riemann sheets.

It is nowadays recognized that the scalar sector of hadronic particles is not well described by the ordinary $q\bar{q}$ picture based on a simple representation of $SU(3)$ flavour symmetry. One very simple reason is the mere fact that the number of physical resonances is much larger than the number of states that can be constructed within a $q\bar{q}$ picture. For instance, in the scalar-isovector sector it is possible to build up only one such state, though two isotriplets are definitely established, the resonances $a_0(980)$ and $a_0(1450)$ [1].

The extended Linear Sigma Model includes (pseudo)scalar as well as (axial-)vector states [2,3]. In this model, the scalar-isovector state is identified with the resonance $a_0(1450)$. In this report, we use the parameters of Ref. [3] in order to calculate the propagator of $a_0(1450)$: in this way we can test the effect of loops on this broad scalar state. Then, we focus on the region below the $K\bar{K}$ threshold and try to find out whether $a_0(980)$ emerges as a companion pole in the propagator.

For our purpose it is sufficient to give only the relevant interaction part of the Lagrangian for the neutral state a_0^0:

$$\mathcal{L}_{\text{int}} = Aa_0^0\eta\pi^0 + Ba_0^0\eta'\pi^0 + Ca_0^0(K^0\bar{K}^0 - K^-K^+)\,, \quad (1)$$

where π^0, η, η', K are the pseudoscalar mesons, and the constants A, B, C are combinations of the coupling constants and masses taken from Ref. [3]. They are constructed in such a way that the decay amplitude for each channel, $-i\mathcal{M}_{ij}$, is momentum independent. The optical theorem for Feynman diagrams can then be applied to compute the imaginary part of the corresponding self-energy loop $\Pi_{ij}(s)$, regularized by a Gaussian 3d-cutoff function with cutoff scale $\Lambda = 0.85$ GeV:

$$\int \mathrm{d}\Gamma\, |-i\mathcal{M}_{ij}|^2 = \sqrt{s}\,\Gamma_{ij}^{\text{tree}}(s) = -\,\mathrm{Im}\,\Pi_{ij}(s)\,, \quad (2)$$

where $\Gamma_{ij}^{\text{tree}}$ is the tree-level width coming from the model and $\mathbf{k}$ is the three-momentum of one of the emitted particles in the decay of the a_0^0 in its rest frame. The real part is obtained by the dispersion relation

$$\mathrm{Re}\,\Pi_{ij}(s) = \frac{1}{\pi}\fint \mathrm{d}s'\,\frac{\mathrm{Im}\,\Pi_{ij}(s')}{s - s'}\,. \quad (3)$$

After that, the self-energy is analytically continued to complex values, $s \to z$, while the continuation into the appropriate unphysical Riemann sheet(s) can be done by adding the discontinuities for each channel,

$$\Pi_{ij}^c(z) = \Pi_{ij}(z) + \text{Disc}\,\Pi_{ij}(z)\,, \quad (4)$$

where $\text{Disc}\,\Pi_{ij}(s) = 2i\lim_{\epsilon\to 0^+}\mathrm{Im}\,\Pi_{ij}(s + i\epsilon)$ and the superscript c indicates the continued function on the next sheet. Note that the appropriate sheet is taken to be the one closest to the physical region.

The complex propagator pole on the sheet nearest to the physical region has coordinates $\sqrt{s} = (1.412 - i0.141)$ GeV, hence a decay width of $\Gamma = 282$ MeV (in good agreement with both the tree-level result from our model and the experiment) and a mass of 1.412 GeV. While the (bare) mass $M_0 = 1.363$ GeV coming from the eLSM differs from the experimental value by at least ~ 50 MeV, the pole mass (as the real part of the propagator pole) lies within the experimental error. Thus, the inclusion of loops represents an improvement of the tree-level results. However, all in all, the loop contributions have just a minor influence on the tree-level values: this is important because it confirms that the fit of Ref. [3] is robust. One should perform this check for all other broad states entering in the eLSM.

Another interesting observation is the fact that we do *not* find a companion pole of $a_0(1450)$: the resonance $a_0(980)$ does not emerge for the values of the parameters determined in Ref. [3]. This result is robust upon variations of the parameters. As a possible outlook for future work one should try to include the $a_0(980)$ as a tetraquark state into the eLSM and/or perform a full scattering analysis so as to investigate the emergence of this resonance in more detail.

References

[1] J. Beringer *et al.* (Particle Data Group), *Phys. Rev.* **D86**, 010001 (2012)

[2] S. Janowski, D. Parganlija, F. Giacosa and D. H. Rischke, *Phys. Rev.* **D84**, 054007 (2011) [http://arxiv.org/abs/arXiv:1103.3238]

[3] D. Parganlija, P. Kovacs, G. Wolf, F. Giacosa and D. H. Rischke, *Phys. Rev.* **D87**, 014011 (2012) [http://arxiv.org/abs/arXiv:1208.0585]

*Work supported by HIC for FAIR, F&E Frankfurt and HGS-HIRe. Presented at the Workshop "Excited QCD 2014", Bjelašnica Mountain, Sarajevo, Bosnia–Herzogovina, February 2–8, 2014. Full version to be published in *Acta Phys. Polon. B Proceed. Suppl.* **7** in 2014.

 doi:10.15120/GR-2014-1-THEORY-24

In-Medium strangeness dynamics at $\overline{\text{P}}$ANDA*

T. Gaitanos[1] *and H. Lenske*[1,2]

[1]Inst. für Theor. Physik, Universität Giessen, Germany; [2]GSI Darmstadt, Germany

Hypernuclear physics opens a unique opportunity to explore the hyperon-nucleon (YN) and the hyperon-hyperon (YY) in-medium interactions at terrestrial laboratories. Such studies are important for a better understanding of the in-medium interactions with strangeness degree of freedom, which is still uncertain, but of relevance for nuclear astrophysics [1]. The experimental knowledge on multi-strangeness hypernuclei has been so far scarce. However, recent experiments at GSI are very promising. In the HypHI [2] experiment precise production rates of single-Λ ($S=-1$) hypernuclei were measured. An abundant production of double-Λ ($S=-2$) clusters is also expected in the $\overline{\text{P}}$ANDAexperiment [3] at FAIR.

We investigate theoretically the multi-strangeness dynamics within the Giessen-BUU (GiBUU) approach [4]. In particular, we have studied antiproton-induced reactions allowing for reactions of the secondary Ξ-beam on a second target. The formation of double-Λ hypernuclei occurs in the Ξ-interaction with the second target [5]. Two issues are of importance for the production of double-strangeness hypermatter, see Fig. 1. At first, the absorption of the Ξ-beam inside the target matter decreases with increasing energy. This is due to the strong decrease of the elementary $\Xi N \rightarrow \Lambda\Lambda$ channel [5]. Secondly, the abundance of bound Λ-hyperons also strongly decreases with rising incident Ξ-energy. This is mainly due to the repulsive vector field which becomes more pronounced as the particle energy increases. These effects lead to a rather strong energy dependent rise of the double-Λ hypernuclear production cross section. Thus low-energetic cascade beams should be used at $\overline{\text{P}}$ANDAin order to obtain high production rates of double-strangeness hyperfragments [5].

So far bare interactions for elementary YN, YY-channels have been used in transport approaches. However, at $\overline{\text{P}}$ANDAthe strangeness dynamics takes place at densities closely up to saturation. We have studied in-medium effects on various YN-processes by solving the Lippmann-Schwinger equation with a Pauli-exclusion operator for intermediate states as the leading-order in-medium effect [6, 7]. The elementary YN cross sections are indeed influenced by in-medium effects, in particular, at low energies, as shown in Fig. 2 (similar effects occur for quasi-elastic channels with strangeness exchange).

In the S=-2 sector the situation is still very controversial theoretically [8]. Presently we are investigating the influence of various calculations on S=-2-channels [9] on the strangeness production in $\bar{p}$-induced reactions and extending our studies to the S=-3 sector by accounting for the formation of Ω-baryons [10]. The preliminary results are very promising concerning a possible formation of multi-strangeness bound systems at $\overline{\text{P}}$ANDA. We emphasize the relevance of our theoretical results for the future activities at FAIR.

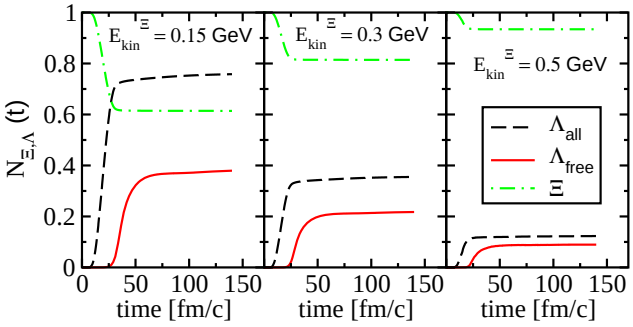

Figure 1: GiBUU results for the time dependence of all and free Λs and of Ξs for central Ξ-induced reactions on Cu-target at beam energies as indicated [5].

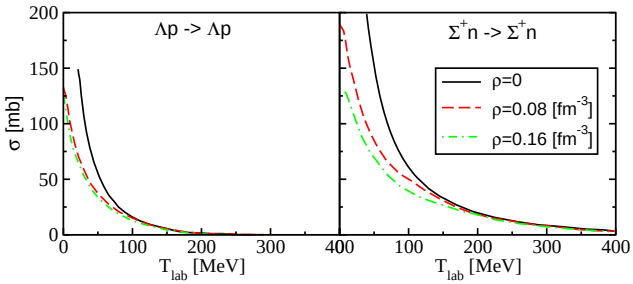

Figure 2: . Energy dependence of elastic in-medium cross sections for ΛN and ΣN scattering at various densities as indicated [7].

References

[1] J. Schaffner, I. Mishustin, Phys. Rev. C53 (1996) 1416.

[2] C. Rappold, *et al.*, Nucl. Phys. A622 (2010) 231.

[3] A.S. Lorente, *et al.*, Phys. Lett. B 697 (2011) 222.

[4] O. Buss, *et al.*, Phys. Rep. 512 (2012) 1.

[5] T. Gaitanos, *et al.*, Nucl. Phys. A881 (2012) 240.

[6] T. Gaitanos, *et al.*, Nucl. Phys. A914 (2013) 405.

[7] A. Obermann, Masters Thesis, 2011, Univ. Giessen, unpublished.

[8] J.K. Ahn, *et al.*, Phys. Lett. B 633 (2006) 214.

[9] T.A. Rijken, Y. Yamamoto, nucl-th/0608074; Y. Fujiwara, *et al.*, Phys. Rev. C64 (2001) 054001.

[10] T. Gaitanos, *et al.*, in preparation.

*Work supported by BMBF, DFG, HIC for FAIR, and GSI-JLU Giessen collaboration agreement

Charmonium production in $\bar{p}$A reactions at threshold*

Alexei Larionov[1,2], *Marcus Bleicher*[1,3], *Albrecht Gillitzer*[4], *and Mark Strikman*[5]

[1]Frankfurt Institute for Advanced Studies (FIAS), D-60438 Frankfurt am Main, Germany; [2]National Research Centre "Kurchatov Institute", 123182 Moscow, Russia; [3]Institut für Theoretische Physik, J.W. Goethe-Universität, D-60438 Frankfurt am Main, Germany; [4]Institut für Kernphysik, Forschungszentrum Jülich, D-52425 Jülich, Germany; [5]Pennsylvania State University, University Park, PA 16802, USA

Charmonium formation reactions on a proton at rest, $\bar{p}p \to R$ ($R = J/\Psi,\ \Psi',\ \chi_c$ etc.), proceed at the beam momentum $p_{\rm lab} = 4 - 6$ GeV/c. Replacing the proton by a nuclear target one gets a good possibility to explore the interactions of the charmonium with nucleons [1, 2]. The preference of the antiproton- to other hadron- and photon-induced charmonium production reactions on nuclei is in the slowness of the produced charmonium. Thus, its formation length is small [2]. On the other hand, nuclear Fermi motion reduces the cross section strongly, $\sigma_{\bar{p}A\to R(A-1)^*} \sim (10^{-4}-10^{-3})Z\sigma_{\bar{p}p\to R}$ at the on-shell peak [2], and broadens the beam momentum region by $\sim \pm p_{\rm lab}p_F/m$, where $p_F \simeq 0.3$ GeV/c is the Fermi momentum and $m = 0.938$ GeV is the nucleon mass.

The eikonal approximation is well suited to study the $\bar{p}A \to R(A-1)^*$ reactions by two reasons: (i) close to the on-shell peak the $\bar{p}p \to R$ formation cross section is large and dominates over other charmonium production channels, and (ii) typical transverse momentum transfers in the formation reaction ($\sim p_F$) and in the charmonium rescattering processes ($\sim 1/\sqrt{B_{RN}} \simeq 0.6$ GeV/c) are much smaller than $p_{\rm lab}$. Within the Glauber model the charmonium production cross section on a nucleus can be calculated as

$$\sigma_{\bar{p}A\to R(A-1)^*} = \int d^2b\, v_{\bar{p}}^{-1} \int_{-\infty}^{\infty} dz \mathrm{e}^{-\int_{-\infty}^{z} dz'\rho(z',b)\sigma^{\rm inel}_{\bar{p}N}} \times \Gamma_{\bar{p}\to R}(z,b)\mathrm{e}^{-\int_{z}^{\infty} dz'\rho(z',b)\sigma_{RN}(z'-z)}, \quad (1)$$

where

$$\Gamma_{\bar{p}\to R}(z,b) = \int \frac{2d^3p}{(2\pi)^3} v_{\bar{p}p}\sigma_{\bar{p}p\to R} f_p(z,b,\mathbf{p}) \quad (2)$$

is the in-medium antiproton width with respect to charmonium R production. $v_{\bar{p}p} = (s(s-4m_N^2))^{1/2}/2E_{\bar{p}}E_p$ is the antiproton-proton relative velocity. $v_{\bar{p}} = p_{\rm lab}/E_{\bar{p}}$ is the antiproton velocity in the target nucleus rest frame. $f_p(z,b,\mathbf{p}) \simeq \Theta(p_{F,p}-p)$ is the proton phase space density with $p_{F,p} = (3\pi^2\rho_p(z,b))^{1/3}$ being the local proton Fermi momentum. Exponential factors in (1) take into account the absorption of incoming antiproton by its inelastic collisions (annihilations mostly) and the absorption of the outgoing charmonium due to its dissociation on the target nucleon ($J/\Psi N \to \Lambda_c\bar{D}$). The corresponding cross sections are $\sigma^{\rm inel}_{\bar{p}N}$ and $\sigma_{RN}(z'-z)$. In the latter case we have checked that taking into account the formation length according to the color diffusion model [2] ($l_{J/\Psi} \simeq 0.4$ fm at $p_{\rm lab} = 4$ GeV/c) has practically no effect on the numerical results. In Fig. 1, the curves have been calculated with

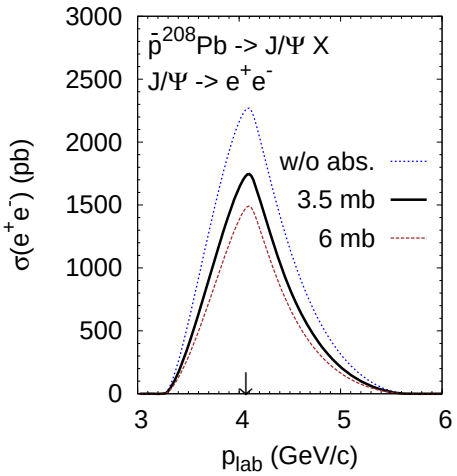

Figure 1: Beam momentum dependence of J/Ψ production cross section on ^{208}Pb. Vertical arrow: $p_{\rm lab} = 4.07$ GeV/c for on-shell J/Ψ production on proton target.

the three values of the $J/\Psi N$ dissociation cross section: $\sigma_{J/\Psi N} = 0,\ 3.5$ and 6 mb. The last two values represent the major uncertainty known from different analyses of J/Ψ production in photon-, hadron- and nucleus- induced reactions on nuclei. The J/Ψ production cross sections are sensitive to the selected values of $\sigma_{J/\Psi N}$ on the level of $\sim 20\%$. For lighter nuclei the sensitivity to $\sigma_{J/\Psi N}$ is reduced. Hence, the transparency ratio analysis can be done for different nuclei to determine the $J/\Psi N$ dissociation cross section (see [3] for details). This analysis can be performed in the future PANDA experiment.

References

[1] S.J. Brodsky and A.H. Mueller, Phys. Lett. B **206**, 685 (1988).

[2] G.R. Farrar, L.L. Frankfurt, M.I. Strikman, H. Liu, Nucl. Phys. B **345**, 125 (1990).

[3] A.B. Larionov, M. Bleicher, A. Gillitzer, M. Strikman, Phys. Rev. C **87**, 054608 (2013).

* Work supported by HIC for FAIR.

 doi:10.15120/GR-2014-1-THEORY-26